Oncogene inactivation-induced senescence facilitates tumor relapse

Philipp Schmitt[1,2,3], Katrin Hönig[1], Ana Milojkovic[1,4], Kathleen Anders[1,5], Evelin Schröck[6], Sascha Sauer[7], Bora Uyar[8], Altuna Akalin[8], Inmaculada Martínez-Reyes[1,9,10,11*], Thomas Blankenstein[1,12*]

[1] Max-Delbrück Center for Molecular Medicine in the Helmholtz Association, Molecular Immunology and Gene Therapy, Berlin, 13125, Germany.
[2] Institute of Immunology, Charité – Universitätsmedizin Berlin, Campus Buch, Berlin, 13125, Germany.
[3] Berlin Institute of Health at Charité – Universitätsmedizin Berlin, BIH Biomedical Innovation Academy, BIH Charité Clinician Scientist Program, Charitéplatz 1, 10117 Berlin, Germany.
[4] Current address: ImmunoScape Pte Ltd, Singapore 228208, Singapore.
[5] Current address: Department of Pediatric Oncology and Hematology, Charité – Universitätsmedizin Berlin, 13353, Berlin, Germany.
[6] Institute for Clinical Genetics, TU Dresden, Dresden, 01307, Germany.
[7] Berlin Institute of Health at Charité – Universitätsmedizin Berlin, Core Facility Genomics, and Max Delbrück Center for Molecular Medicine in the Helmholtz Association Max Delbrück Center for Molecular Medicine, Berlin, 13125, Germany.
[8] Max-Delbrück Center for Molecular Medicine in the Helmholtz Association, Bioinformatics and Omics Data Science Platform, Berlin, 13125, Germany.
[9] Department of Hematology, Oncology and Cancer Immunology, Campus Benjamin Franklin, Charité - Universitätsmedizin Berlin, corporate member of Freie Universität Berlin and Humboldt-Universität zu Berlin, 12203 Berlin, Germany.
[10] German Cancer Research Center, Heidelberg, Germany.
[11] German Cancer Consortium (DKTK), partner site Berlin, a partnership between DKFZ and Charité-Universitätsmedizin Berlin, 10117 Berlin, Germany.
[12] Berlin Institute of Health at Charité – Universitätsmedizin Berlin, 10117 Berlin, Germany.

*These authors contributed equally to this work. Correspondence should be addressed to: blanke@mdc-berlin.de, imreyes@mdc-berlin.de

SUMMARY

Oncogene-targeted therapy has emerged as a promising avenue for delaying tumor progression. However, patients often develop drug resistance and early tumor recurrence. We analyzed the effects of oncogene inactivation *in vitro*, and identified the induction of senescence and metabolic reprogramming as two major adaptive mechanisms. *In vivo*, we observed that senescent cells exhibited an increased propensity for tumor relapse, accompanied by notable chromosomal abnormalities and the acquisition of alternative oncogenic pathways. Oncogene inactivation-induced senescence rendered cells reliant on autophagy, making them more susceptible to autophagy inhibition *in vitro*. However, combining oncogene inactivation with autophagy-targeted senolysis *in vivo* in immunocompetent mice, unexpectedly facilitated tumor growth compared to oncogene inactivation alone. Similarly, oncogene inactivation in established tumors followed by autophagy inhibition led to increased tumor relapse in immunodeficient mice compared to the placebo group. Our results underscore senescence as a main mechanism allowing cancer cells to survive oncogene deprivation. Oncogene inactivation-induced

senescence induces genetic abnormalities and is a main driver of tumor relapse. Our results suggest different metabolic dependencies of senescent cells *in vitro* and *in vivo* and underscore the importance of evaluating potential drug candidates in relevant preclinical mouse models, as therapeutic effects observed *in vitro* may not necessarily translate to meaningful clinical outcomes *in vivo.*

INTRODUCTION

In recent years, oncogene-directed therapy has emerged as a promising approach in cancer pharmacological research. However, despite its potential, clinical efficacy is often hampered by the development of drug resistance and early cancer relapse.[1–4] The mechanisms enabling cancer cells to adapt to the inactivation of oncogenes, to sustain a dormant state before tumor relapse and to trigger the resurgence of cancer cell proliferation are not completely understood. In this study, we seek to investigate these processes using a mouse tumor model in which cancer cell proliferation is driven by the oncogene SV40 large T antigen (Tag) in an inducible manner allowing us to activate and inactivate the oncogene *in vitro* and *in vivo*. Our results show that oncogene inactivation leads to the acquisition of cellular senescence and induction of a pro-inflammatory senescence-associated secretory phenotype (SASP). Senescence is widely defined as a durable form of growth arrest and is linked to extensive cellular stress that can be induced by different kind of insults, including oncogenic activation, radiation or chemotherapy.[5] Since the first description by Hayflick in 1961[6], the understanding of cellular senescence has evolved dramatically and an increasing body of literature deals with its beneficial as well as its detrimental role on health, ageing and disease.[7–9] In the context of cancer therapy, therapy-induced senescence (TIS) had been mainly described as a tumor suppressive mechanism by limiting the propagation of genetically unstable cancer cells and keeping tumor growth in check. Therefore, it was regarded as a favorable outcome of therapy for a long time.[10] However, several studies indicate that TIS and the SASP might have tumor-promoting effects.[11–13] Importantly, it has been shown that cancer cells are capable of escaping the TIS, often in an even more aggressive form.[14,15] Therefore, the use of senolytic drugs aimed at targeting residual senescent cancer cells after targeted therapy was proposed as a promising therapeutic strategy. Most senolytic drugs are designed to selectively eliminate or induce cell death in senescent cells by targeting key proteins involved in apoptosis. In recent studies, novel senolytics have been developed to target additional vulnerabilities of senescent cells, including their altered metabolism. For instance, in a mouse lymphoma model, therapy-induced senescent cells were successfully targeted pharmacologically, exploiting their plurimetabolic state and heightened autophagy. This intervention resulted in significant anti-tumor therapeutic effects.[16]

To date, most research on senescence in cancer has primarily focused on senescence triggered by radiation or DNA-damaging chemotherapy. In this study, we focused on senescence as an adaptive mechanism to oncogene deprivation and examined the role of oncogene inactivation-induced senescence in tumor development. Importantly, because oncogene expression is reversible in our model, we can simulate therapy-induced senescence (TIS) by inactivating the oncogene and mimic disease progression after therapy failure by restarting proliferation following prolonged oncogene inactivation-mediated senescence. Our findings indicate that oncogene inactivation and the accompanying senescence phenotype are necessary for tumor relapse and are associated with worse disease progression and outcomes.

Relapsed tumors exhibited notable chromosomal abnormalities and acquired alternative oncogenic pathways. We identified p53 inactivation through upregulation of MDM2 as a mechanism contributing to the maintenance of genomic instability, likely facilitating escape from senescence and subsequent tumor growth *in vivo*. Interestingly, we found that oncogene inactivation-induced senescence reprograms cellular metabolism and makes cells dependent on autophagy for survival *in vitro*. By targeting autophagy, we could specifically eliminate senescent cancer cells (senolysis) *in vitro*. However, to our surprise, combining oncogene inactivation with autophagy-targeted senolysis *in vivo* accelerated tumor relapse. These results suggest significant differences in the metabolic dependencies of senescent cells *in vitro* and *in vivo*. Moreover, our findings indicate that autophagy acts as a tumor suppressor in senescent cells that survive oncogene deprivation. This insight is crucial for the strategic design of anti-cancer sequential and combinatorial therapies, suggesting caution in targeting autophagy as part of these therapeutic approaches.

RESULTS

TagLuc inactivation induces senescence and SASP.

To study the mechanisms enabling cancer cells to adapt to the inactivation of oncogenes, we used cancer cells isolated from tumors that grew sporadically in transgenic mice.[17,18] Specifically, we used cells from a gastric carcinoma (clone 4) and from a spindle cell sarcoma isolated from the snout (TTC#3055). This established transplantable tumor cell lines express the oncogene SV40 large T antigen fused to the reporter gene firefly luciferase (TagLuc) under the tetracycline response element (TRE) along with the rtTA2S-M2 transactivator (rtTA). In clone 4 cells, the loxP-flanked stop cassette was excised by transient gene transfer in cultured cells with a Cre recombinase-encoding adenovirus. This system allows activation or inactivation of the oncogene by adding or withdrawing doxycycline (dox), respectively, *in vitro* and *in vivo* as well as the monitoring of tumor cell growth *in vivo* by bioluminescence imaging upon subcutaneous transplantation of these cells (Figure 1A).[17] Hence, this model provides an ideal setting to analyze the effects of oncogene inactivation by withdrawing dox on cancer cells *in vitro* and on tumor development *in vivo*. First, we confirmed loss of TagLuc expression (oncogene inactivation) as early as one day after dox deprivation in clone 4 and in TTC#3055 cells (Figure 1B and Extended Data Figure 1A). Inactivation of TagLuc inhibited cell proliferation (Figure 1C) and resulted in cell death in most of the cultured clone 4 cells, with approximately 23% of the original population remaining alive (Extended Data Figure 1B). Upon oncogene inactivation, cells progressively exhibited cell cycle arrest (Figure 1D). Cells became enlarged in size and showed a flattened and irregular shaped phenotype characteristic of cells with a senescence phenotype (Figure 1E and Extended Data Figure 1C). Seven days after TagLuc inactivation, a significant increase in senescence-associated β-galactosidase (SA-β-gal) expression could be detected in clone 4 cells (Figure 1E). We further analyzed the expression levels of *Cdkn1a* (previously known as p21) and *Cdkn2a* (previously known as p16), proteins required for the senescence induction and typically found to be upregulated in senescent cells.[19] Our results showed increased mRNA levels of *Cdkn1a*, and downregulation of *Cdkn2a* after TagLuc inactivation (Extended Data Figure 1D) suggesting that cells are dependent on *Cdkn1a* but not *Cdkn2a* to acquire a senescence phenotype following TagLuc inactivation. Tag-mediated inhibition of the phosphorylation of the retinoblastoma protein (pRB1) is known to upregulate p16 expression in proliferating cancer cells[20], therefore we reasoned that loss of Tag and the subsequent activation of pRB1 leads to a downregulation of p16 in the senescent

state. A prominent feature of senescent cells is the formation of a SASP.[12] Following the induction of senescence, cells initiate the secretion of cytokines and growth factors. Recent advancements have highlighted the considerable heterogeneity of the SASP, with its composition influenced not only by the cell type but also by the specific mechanism triggering senescence induction.[21,22] To analyze the SASP, we generated conditioned medium of proliferating (TagLuc expressing) and senescent (TagLuc non-expressing) clone 4 cells. Using a semi-quantitative cytokine array, we observed an increase in the secretion of interleukin 6 (Il-6), matrix metalloprotease 2 (Mmp2) and Mmp3 in senescent cells (Extended Data Figure 1E). Elevated levels of Il6 and Mmp3 secretion upon senescence induction were further verified using an enzyme-linked immunosorbent assay (ELISA) (Figure 1F). Overall, the morphological features, the expression of SA-β-gal, the G0/G1 arrest as well as the SASP confirm the acquisition of senescence upon oncogene inactivation.

TagLuc inactivation-mediated senescence promotes major transcriptomic changes and the acquisition of a plurimetabolic state.

To further analyze the phenotype of oncogene inactivation-mediated senescence, we performed mRNA sequencing on clone 4 cells in two states: proliferating (TagLuc expressing, +dox) and senescent (not expressing TagLuc, -dox). We then compared the differentially expressed genes. The results show major transcriptional changes with 1067 genes significantly overexpressed (p-adj < 0.001 and log2-fold-change > 2) and 928 genes downregulated (p-adj < 0.001 and log2-fold-change < -2) in senescent cells compared to proliferating cells (Extended Data Figure 2A, Supplementary Document 1). Gene set enrichment analysis revealed pathways related to the regulation of the cell cycle and mitotic processes amongst the downregulated ones in senescent cells, in accordance with the inhibition of proliferation and cell cycle arrest previously observed (Figure 2A). The pathways identified among the top upregulated ones include keratan sulfate degradation, ECM-receptor interaction, and collagen degradation, suggesting significant remodeling of the extracellular matrix in senescent cells. (Figure 2B). Remodeling is further supported by the upregulation of pathways related to extracellular matrix organization and degradation of the extracellular matrix (Figure 2B). The activation of pathways like cytokine-cytokine receptor interaction and complement and coagulation cascades indicates an inflammatory profile in senescent cells (Figure 2B). In accordance with the higher SASP displayed by oncogene-deprived cells, genes associated with it were found upregulated in senescent cells (Extended Data Figure 2B). Notably, using the cancer single-cell state atlas (CancerSEA) database we further confirmed the downregulation of pathways regulating the cell cycle, DNA repair, DNA damage and proliferation in senescent cells (Figure 2C and Extended Figure 2C).[23] Interestingly, pathways critical to tumor development—such as hypoxia, angiogenesis, invasion, and inflammation—were enriched in senescent cells (Figure 2D and Extended Figure 2D). Additionally, the involvement of sphingolipid metabolism and regulation of insulin-like growth factor (IGF) transport and uptake by insulin-like growth factor binding proteins (IGFBPs) indicates metabolic reprogramming and altered growth factor signaling in senescent cells (Figure 2B). We subsequently analyzed the metabolic features of proliferating and senescent clone 4 cell. Our analysis of the metabolic features revealed that senescent cells display a higher basal glycolytic rate compared to proliferating cells, as well as higher compensatory glycolysis following mitochondrial inhibition (Fig 2E and Extended Figure 2E). Likewise, basal, coupled, and maximal respiration rates were all

increased in senescent cells compared to proliferating cells (Figure 2F and Extended Figure 2F). These results indicate that senescent cells acquire a plurimetabolic state.

Oncogene inactivation-induced senescence predisposes to cancer relapse.
Next, we studied the effects of oncogene inactivation and the acquired senescence phenotype on disease progression *in vivo*. As a control, we injected proliferating (TagLuc expressing, +dox) clone 4 cells in immunocompetent transgenic CM2 mice expressing the rtTA to avoid an immune response against the transactivator. Clone 4 cells were also injected into immunodeficient (Rag2-KO) mice.[17] The mice received dox-supplemented drinking water to ensure continuous oncogene expression (Extended Data Figure 3A). After an initial phase of tumor growth, tumors were rejected by anti-Tag-specific T cells in immunocompetent mice, while tumors progressively grew in Rag2-KO mice (Extended Figure 3B-D). Of note, we could not observe any tumor relapse in this group over the observation period of 300 days. To study the effect of senescence on disease progression *in vivo*, we inactivated TagLuc by withdrawing dox *in vitro* for 14 days and inoculated senescent clone 4 cells in CM2 and Rag2-KO mice. After a period of 4 weeks, in which cells remained in a dormant state without TagLuc expression, dox was added to the drinking water to reactivate the oncogene expression (Figure 3A-C, transient senescence experimental conditions). Similarly, as observed with proliferating cells, after an initial phase of tumor growth, tumors regressed only in CM2 mice following senescent cell inoculation and tumor growth induction due to immune-mediated killing (Figure 3B,C and Extended Figure 3E). Interestingly, we observed tumor relapse in 9 out of 9 mice after a long latency period (Figure 3D). We observed similar outcomes when oncogene-deprived senescent TTC #3055 cells were injected, wherein relapsed tumors occurred subsequent to an initial regression of tumors in immunocompetent hosts (Figure 3E,F). These data indicate that a short transient senescent state dramatically predisposes to relapse (Figure 3G). Additionally, we injected senescent clone 4 cells in CM2 mice as described above but this time, TagLuc was never reactivated (Figure 3H, persistent senescence experimental conditions). Nevertheless, tumors grew in 10 out of 12 mice after a long latency, further supporting senescence as a facilitator of tumorigenicity (Figure 3I). We re-isolated the tumors and generated cell lines to identify factors contributing to tumor relapse following transient senescence or tumor growth following persistent senescence. We observed that 4 out of 5 of the tested cell lines did not express TagLuc despite continuous proliferation (Extended Data Figure 3F). Consistently, Tag mRNA levels were undetectable in TagLuc-negative re-isolated cell lines (Extended Data Figure 3G). This data indicate that most relapsed tumors lost dependency on TagLuc as cancer-driving oncogene and might have activated an alternative oncogenic pathway.

Cancer cells from relapsed tumors depend on Mdm2 and display polyploidy.
To identify potential alternative oncogenic pathways, we performed mRNA sequencing on the re-isolated cell lines (from relapsed tumors in the transient senescence experimental conditions) and compared gene expression to parental proliferating clone 4 cells (on dox) and senescent clone 4 cells (off dox). We found 143 genes upregulated and 67 downregulated in the cell lines generated from relapsed tumors (Figure 4A). The full dataset can be found in Supplementary Document 2. The upregulation of pathways such as MAPK signaling pathway, cytokine-cytokine receptor interaction and signaling by receptor tyrosine kinases in relapsed tumors indicates a molecular signature associated with enhanced growth factor signaling, cell proliferation, and survival mechanisms (Extended Data Figure

4A). The identified downregulated genes in relapsed tumors are related to cellular structure and extracellular matrix components indicative of alterations in the tumor microenvironment (Extended Data Figure 4B). These downregulated pathways may influence cell-cell interactions, signaling pathways, and tissue organization within the tumor. Among the upregulated genes, we found murine double minute 2 (*Mdm2*) as a potential new oncogenic driver gene (Figure 4B). Mdm2 antagonizes TP53, and therefore, in the absence of Tag, high levels of MDM2 can mimic the cellular and metabolic effects that Tag mediates to inactivate TP53 when expressed. To validate the dependency of isolated tumors on MDM2 activity, we treated two of the relapsed cancer cell lines *in vitro* with the MDM2-inhibitor AMG 232.[24] While proliferation of the parental clone 4 cells remained unaffected, the proliferation of the re-isolated cancer cell lines was significantly diminished, confirming MDM2 upregulation as an alternative oncogenic pathway (Figure 4C). Previous studies have shown that cancer cells that escaped senescence developed poly- and aneuploidy.[25,26] The analysis of the karyotype of cancer cell lines from relapsed tumors after transient and persistent senescence showed dramatic chromosomal abnormalities compared to the parental cell line (Figure 4D-F and Extended Data Figure 4C,D). The parental clone 4 cells (never off-dox) were mostly diploid except for a few amplified chromosomes that were found to be heterogenous among the cells analyzed (Figure 4D and Extended Data Figure 4C). The acquired chromosomal aberrations are likely a consequence of the Tag-mediated inhibition of pRB1 and TP53, which results in genomic instability. The cancer cell lines derived from relapsed tumors, however, showed dramatic and complex chromosomal rearrangements and increased polyploidy, albeit the function of pRB1 and TP53 being restored after Tag inactivation. Overall, the data suggest that a brief period of oncogene inactivation-induced senescence is sufficient to irreversible instill genomic instability in the form of chromosomal polyploidy. The upregulation of an alternative oncogenic pathway together with genomic instability is likely to facilitate cancer cells to escape their senescent phenotype and to resume tumor growth.

Autophagy-targeted therapy has senolytic effects *in vitro*.

In recent years, efforts have been made to identify and exploit drugs with senolytic properties to counteract the tumor-promoting effects of cancer senescence.[27] Metabolism is a vulnerability that could be exploited to selectively target senescent cells. Previously, we demonstrated that the inactivation of TagLuc enhances autophagy, an integral part of the cellular response to changes in metabolic states.[17] Under stress conditions, autophagy plays a crucial role in maintaining cellular homeostasis by removing damaged or unnecessary cellular components. In a myc-driven lymphoma model, blocking autophagy resulted in the selective elimination of senescent cells.[16] We hypothesized that the inhibition of autophagy after TagLuc inactivation could selectively eliminate senescent cells resulting in long-lasting tumor remission. To test this hypothesis, we treated proliferating (TagLuc expressing, +dox) and senescent (TagLuc non-expressing, -dox) clone 4 cells with the autophagy inhibitor Lys05 *in vitro.*[28] To exclude early oncogene inactivation-mediated apoptosis, clone 4 cells were treated with Lys05 following 14 days of dox deprivation. After treatment with Lys05, we analyzed the distribution of living, apoptotic and dead cells (Figure 5A and Extended Figure 5A). Senescent clone 4 cells exhibited a reduced fraction of living cells before the initiation of treatment, which further decreased in a dose-dependent manner (Figure 5A and Extended Figure 5A). In contrast, proliferating (TagLuc expressing) clone 4 cells demonstrated lower sensitivity to Lys05 treatment (Figure 5A and Extended Figure 5A). These results demonstrate

that the pharmacologic inhibition of autophagy has specific senolytic effects on oncogene-deprived cells *in vitro*. We knocked down Beclin-1, a protein involved in regulating autophagy, in Tet-TagLuc cells. Unlike clone 4 cells, where TagLuc requires dox for expression, in these cells TagLuc is expressed in the absence of dox, facilitating cell proliferation. Of note, in Tet-TagLuc cells, TagLuc expression is lost upon dox treatment.[17] Consistent with our previous findings, 7 days of dox treatment induced the loss of TagLuc expression in cells transduced with a shRNA control, accompanied by a rapid shift of LC3 from a soluble to a membrane-bound form (LC3-II), indicative of activated autophagy (Figure 5B and Extended Figure 5B). Beclin-1 downregulation in two independent Tet-TagLuc clones, combined with oncogene inactivation, abrogated the increase in LC3-II, preventing autophagy activation and leading to cell death (Figure 5B,C and Extended Figure 5B,C). Downregulation of procaspase-3 expression upon silencing of Beclin-1 confirmed apoptotic-mediated cell death in oncogene-deprived cells unable to use autophagy as a survival pathway (Extended Data Figure 5E). These results confirm that both the genetic and pharmacologic inhibition of autophagy promote apoptosis of cells displaying oncogene deprivation-mediated senescence *in vitro*.

Autophagy-targeted therapy facilitates tumor relapse

Subsequently, we sought to study the effect of Lys05 in targeting senescent cells *in vivo*. First, we analyzed the sensitivity of proliferating (TagLuc expressing, +dox) clone 4 cells to Lys05 treatment *in vivo* (Extended Data Figure 5F). Clone 4 cells expressing TagLuc (growing on dox) were injected into Rag2-KO mice, which were continuously given dox in the drinking water. After one week, mice were treated with Lys05 via intraperitoneal (i.p.) injection at a final concentration of 20 mg/kg or with placebo (PBS, 4% DMSO), respectively, for a total of six dosages. The treatment was divided up into 2x3 dosages, separated by a one-week interval. An intermittent dosing regimen was chosen, as studies showed that intermittent administration of senolytics is as effective as continuous dosing but is less likely to cause off-target and side effects.[29,30] We found that consistent with our results *in vitro*, targeting autophagy had no major effect on tumor growth in Rag2-KO mice (Extended Data Figure 5G). To study whether Lys05 treatment would prevent tumor growth of senescent cells with no oncogene induction (persistent senescence), we injected clone 4 cells 14 days after TagLuc inactivation *in vitro* into immunocompetent mice that were kept without dox treatment. One week after inoculation, mice were treated with Lys05 or left untreated (Figure 5D). To our surprise, Lys05-treated mice showed accelerated tumor growth and tumors were significantly bigger in size in the Lys05 treated group 95 days after tumor cells injections (Figure 5E,F). To better mimic therapy induced regression of tumors and analyze the effect of inhibiting autophagy upon senescence induction we established tumors in immunodeficient mice and withdraw dox after 10 weeks to inactivate the oncogene. We next treated mice with Lys05 to target cells that acquired a senescent state after oncogene inactivation (Figure 5G). Similar to the persistent senescence experimental conditions, Lys05 failed to selectively target senescent cells after oncogene inactivation *in vivo* and rather facilitated tumor relapse (Fig 5H). At day 98 post tumor injections, tumors in the Lys05 group were significantly bigger than tumors in the placebo group (Fig. 5I). In summary, whereas senescent cancer cells are more susceptible to autophagy inhibition *in vitro*, oncogene inactivation in combination with autophagy-targeted senolysis facilitated tumor growth or relapse.

DISCUSSION

In this study, we analyzed the effects of oncogene inactivation *in vitro* and found that the acquisition of cellular senescence accompanied by a pro-inflammatory SASP and metabolic alterations are key adaptive mechanisms. Other chemotherapeutic agents and the inactivation of c-Myc have also been shown to induce senescence and have been proposed as mechanisms of tumor regression and therapy resistance[31–33]. Our results show that *in vivo*, oncogene inactivation-induced senescence has major effects on disease progression. Notably, we observed that oncogene inactivation-induced senescence predisposes to tumor relapse of previously regressed tumors resulting in significantly worse prognosis. Several factors are likely involved in driving this phenotype. We observed that upon oncogene inactivation-induced senescence, cells activate the SASP, a complex network of factors known to induce a pro-inflammatory, angiogenetic milieu which can promote tumor growth.[12] In addition, chemotherapy-induced senescence has been shown to cause polyploidy in cancer cells, allowing them to resume proliferation despite their senescent state.[26,34] Interestingly, results showed that cancer cells undergoing senescence without polyploidy were unable to escape their senescent state.[35] In our model, cancer cells re-isolated from relapsed tumors, where senescence was transiently induced, displayed severe polyploidy. This phenotype mimics clinical observations, as many human cancer cells undergo dramatic chromosomal amplification, contributing to tumor progression and therapy resistance.[36] Acquired polyploidy likely contributes to bypassing the senescent phenotype by fostering the acquisition of alternative oncogenic pathways. Indeed, we observed an upregulation of Mdm2 expression in cancer cells re-isolated from relapsed tumors. Mdm2 functions by antagonizing p53 and is frequently overexpressed in various tumor types.[37] Drug-mediated inhibition of Mdm2 using AMG 232 resulted in a significant reduction in the viability of cancer cells re-isolated from relapsed tumors. Our findings indicate that the functional inactivation of p53 is essential for the proliferation of former senescent cancer cells, exhibiting polyploidy and high genomic instability. In a related study, transgenic myc-dependent lymphomas, upon undergoing senescence following myc inactivation, eventually reverted to a proliferative state by restoring myc activity, achieved through mutations in the tetracycline transactivator or genomic rearrangements.[38] In our model, upregulation of Mdm2 mimics the effect of TagLuc, as both oncogenes result in p53 inactivation. Further investigations are required to determine the specific pathways and mechanisms that are necessary and sufficient to compensate oncogene addiction and allow senescence escape following oncogene inactivation.

Previous research has suggested that a 'two hits' therapy approach, focused on treating senescence following first-line treatment, could potentially improve cancer treatment outcomes.[27] In this approach, the initial cancer burden is reduced through conventional anti-cancer therapies. Cells that survive these treatments often undergo therapy-induced senescence (TIS) and could be selectively eliminated through a second step involving senescence-targeted therapy. Given the detrimental effects of inducing cellular senescence in cancer cells on tumor progression and relapse, we investigated whether senolytic therapy could prevent tumor formation by eliminating surviving senescent cancer cells after TagLuc inactivation. In a previous study, we observed an upregulation of autophagy following TagLuc inactivation.[17] Autophagy serves as a protective mechanism against cytotoxic stress, shielding cells from programmed cell death.[16] However, several studies have highlighted the context-dependent and sometimes opposing effects of autophagy on tumor cell survival. In advanced cancer, autophagy serves as a mechanism for nutrient supply to rapidly dividing cells, promoting survival within the harsh tumor microenvironment.[39] In

contrast, in the early stages of carcinogenesis, autophagy primarily acts as a cytoprotective control system, limiting oxidative stress and mutations, and thus acting as a barrier against malignant transformation, thereby preventing cancer development.[40] Our results show that autophagy inhibition is highly effective at selectively killing senescent cells *in vitro*. However, to our surprise, targeting autophagy in mice injected with senescent cancer cells with no TagLuc reactivation resulted in a significantly accelerated rate of tumor growth compared to the placebo-treated group in immunocompetent mice. To mimic the two-step approach in our tumor model, we established tumors in immunodeficient mice and subsequently inactivated the oncogene, leading to tumor regression. Mice were then treated with an autophagy inhibitor, which not only failed to eliminate senescent cells but even facilitated relapse compared to the placebo group. This data suggest that the dependency of metabolic pathways largely differs *in vitro* and *in vivo* and that targeting autophagy in senescent cells helped them escape the senescent state. We hypothesize that the blockade of autophagy might disrupt its cytoprotective function and potentially facilitate the acquisition of new mutations. In this context, Was et al. reported that senescent cancer cells treated with chemotherapy, and additionally exposed to a single pulse of bafilomycin A, an autophagy inhibitor with pharmacodynamic properties similar to Lys05, exhibited an increase in the number of polyploid cells and demonstrated a higher capacity to form tumors upon transplantation in NOD/SCID mice.[41] Similarly, a study by Aqbi et al. found that knocking down Atg5, a key gene involved in the autophagy pathway, in ADR-treated breast cancer cells led to earlier tumor recurrence compared to cells with normal autophagy function.[42] These findings suggest that inhibiting autophagy in chemotherapy-treated cancer cells may paradoxically promote tumor recurrence or relapse. Similarly, we show that autophagy is an essential tumor-suppressive mechanism after oncogene inactivation to limit the propagation of genetically unstable polyploid cancer cells.

In conclusion, our study highlights the complexity of translating promising *in vitro* results to *in vivo* settings. This underscores the need for caution in drug discovery, highlighting that positive outcomes observed *in vitro* may not necessarily translate to meaningful clinical outcomes. Therefore, it is crucial to utilize clinically relevant tumor models to evaluate the efficacy of potential anti-cancer drugs, with the goal of reducing the attrition rate of drugs advancing into clinical trials. Although our study focused on oncogene inactivation-induced senescence driven by TagLuc, it is evident that senescence can be induced by various other physiological or pathological stressors.[31–33] Hence, it would be valuable to investigate whether autophagy-targeted therapy yields similar effects in cancers driven by different oncogenes. Furthermore, considering the heterogeneity of senescence, future studies should explore whether the detrimental impact of autophagy-targeted senolysis extends to other forms of senescence induced by diverse stress factors. These investigations will provide critical insights into the broader applicability and potential limitations of autophagy-targeted therapies in cancer treatment.

METHODS

Cell culture and oncogene inactivation

Clone 4 cells, TTC #3055 and TetTagLuc cells were cultured in Dulbecco's modified eagle medium (DMEM, Gibco), supplemented with 10% heat inactivated fetal calf serum (PAN, Biotech) and 50 µg/ml gentamicin (Gibco). Clone 4 and TTC #3055 cells were cultured with 1 µg/ml doxycycline (Sigma) and medium was changed

every 3 days. For oncogene inactivation, clone 4 and TTC #3055 cells were cultured, if not otherwise specified, in dox-free medium for 14 days. TetTagLuc cells were cultured in the presence of doxycycline for oncogene inactivation.

Western blot

Cells were lysed using the mammalian cell lysis kit (Sigma-Aldrich). The protein concentration was determined using the bicinchoninic acid (BCA) assay (Pierce, Rockford, USA). Proteins were separated by SDS-PAGE gels and transferred to nitrocellulose membranes (Amersham, Freiburg, Germany). Antibodies used for western blotting included anti-SV40 T antigen (2,5 µg/ml, clone PAb416, Calbiochem), polyclonal anti-caspase-3 (1:1000; R&D Systems GmbH), polyclonal anti-LC3 (1:1000; Novus Biologicals), and anti-beclin-1 (1:1000, Cell Signaling). Secondary anti-rabbit and anti-mouse IgG antibodies conjugated to HRP were from Southern Biotech, USA. Super Signal chemiluminescent substrate kit (Thermo Fisher) and the LUMI-F1 imaging workstation (Roche) were used to detect chemiluminescence signal. For loading control, membranes were incubated with polyclonal anti-mouse ß-actin (0.2 µg/ml A; Abcam) or monoclonal anti-mouse ß-actin (1:5000; clone AC-15, Sigma-Aldrich).

SA-β-gal staining

Cells were cultured in 6-well plate in the presence or absence of dox until they reached ~50-80% confluency. SA-β-gal was detected using the Senescence Detection Kit (BioVision). In short, cells were fixed with fixation solution for 15min. After washing, cells were stained with a solution containing 1 mg/ml X-gal at 37 °C overnight. The next day, cells were visualized using Olympus FSX100.

Cell cycle analysis

Cells were incubated with 10 µM BrdU (Sigma) for 60 min. Next, cells were washed with PBS and harvested. For permeabilization, cells were resuspended in ice-cold 70% ethanol mixed with PBS and stored for 2 hours at -20°C. Cells were washed again with PBS, incubated with 2 ml 2N HCl/0,5 % Triton X-100 for 30 min, centrifuged and incubated with 2 ml 0.1 M sodium tetraborate (Sigma) for 10 min. After 2 washing steps with PBS, cells were stained with anti-BrdU antibody (Biolegend) supplemented with 0,5% Tween-20 and 1% BSA for 30 min at room temperature. Next, cells were incubated with 20 µg/ml propidium iodide (containing 0,5% Tween-20, 1% BSA and 10 µg/ml RNase A (Qiagen) for 30 min at room temperature. Probes were analyzed via flow cytometry (BD FACS Canto II) and data was analyzed using FlowJo™ v10.8 Software (BD Life Sciences).

Real-time quantitative PCR

Total mRNA was extracted from proliferating, TagLuc expressing and senescent, TagLuc non-expressing clone 4 cells using the RNeasy Mini Kit (Qiagen). 1 µg was reverse-transcribed using an oligo-dT primer and ProtoScript II Reverse Transcriptase (NEB) Kit according to the manufacturer's instructions. The reaction products were diluted (10x) in nuclease free water. 2 µl of the sample was subjected to real-time PCR, which was performed in triplicates using TaqMan probes for the mouse genes CDKN1A, CDKN2A and GAPDH (Applied Biosystems). Expression levels of CDKN1A and CDKN2A relative to that of GAPDH were calculated using the $2^{-\Delta\Delta CT}$ method. The difference of the cycle threshold (CT) of the target and the reference gene was calculated (ΔCT) and compared between the two samples (ΔΔCT). Finally, expression ratio was calculated according to the formula $x = 2^{-\Delta\Delta CT}$.

Cytokine antibody array

Proliferating, TagLuc expressing and senescent, TagLuc non-expressing clone 4 cells were cultured in DMEM for 48h to generate conditioned medium (CM). Cells were counted and CM was filtered and analyzed using Mouse Cytokine Antibody Array C2000 (RayBiotech) according to the manufacturer's protocol. Briefly, array membranes were preincubated with 2 ml of blocking solution. CM was diluted with DMEM to reach volume equivalents of 2 x 10^5 cells/ml. Array membranes were incubated with 1 ml of CM (3h, room temperature), washed, and incubated with biotin-conjugated antibody cocktail (overnight, 4°C). The next day, HRP-Streptavidin was added (2h, room temperature), followed by a washing step of the array membranes and addition of the detection solution. Chemiluminescence was analyzed using the Lumi Imager F1 (Roche) with an exposure time of 1min.

ELISA

Conditioned medium was generated as described above and diluted with DMEM to reach volume equivalents of 2 x 10^6 cells/ml. CM was then analyzed by utilizing the Il6 and Mmp3 mouse ELISA kit (Life Technologies). ELISA was performed according to the manufacturer's instructions.

Luciferase activity assay

Cells were cultured in a 6-well plate, washed with PBS once and incubated with 500 µl of reporter lysis buffer (Promega) for 2 min. A cell scraper was used to harvest the cells and the cell suspension was transferred into Eppendorf tubes. The probes were snap-frozen in liquid nitrogen for 2 minutes, thawed on ice, and centrifuged at 12.000 rpm for 10 min. Protein concentration of the supernatant was determined by NanoDrop (Thermo Scientific). 10 µl of supernatant was mixed with luciferase assay buffer (Promega) and luciferase substrate buffer (Promega), respectively. TagLuc activity was measured using a Mithras LB 940 luminometer (Berthold Technologies) and relative light unit (RLU) was calculated according to total µg protein.

mRNA sequencing and differential expression analysis

mRNA of the proliferating (TagLuc expressing, +dox) and senescent (TagLuc non-expressing, -dox) cancer cells was isolated using the RNeasy Mini Kit (Qiagen). mRNA integrity was measured using the Agilent Tape Station 4200. Probes were then analyzed via HiSeq4000. Differential gene expression analysis was performed as described before (detailed methods can be found in references 43 and 44). In short, sequencing reads were quality-checked and mapped to the mouse genome. Differential expression analysis was performed using the DESeq2 R statistical package. For data analysis, the adjusted p-value was set <0.001 and the minimum log fold change of upregulated genes was set at ≥1. All procedures were performed in triplicates.

Biological term enrichment analysis

Biological term enrichment analysis was carried out using two different methods. gProfiler2 R package (version 0.2.2) as used to detect enriched pathways (annotated as in the KEGG and Reactome databases) or GO terms among significantly upregulated/downregulated genes (as in Figures 2A-B).[45] As a complementary approach, gene-set enrichment analysis was carried out using the fgsea R package (version 1.24.0) with cancer state signature genes downloaded from the CancerSEA database (as in Figure 2C-D).[46,23] For the GSEA analysis, the genes were ranked by

decreasing order of the -log10(p-value) multiplied by the sign of the log2-fold-change of each gene.

Oxygen Consumption Rate and Extra-Cellular Acidification Rate Measurements. The oxygen consumption rate (OCR) and extra-cellular acidification rate (ECAR) were measured using a XF96 extracellular flux analyzer (Seahorse Bioscience). Cells were seeded at a density of 8 x 10^4 (on dox) and 4 x 10^4 (off dox) cells per well on poly-D-lysine (PDL)-treated plates, each well containing 200 µl of Seahorse XF Base Medium supplemented with 1 mM pyruvate, 2 mM glutamine, and 10 mM glucose. The plates were then incubated in a non-CO_2 incubator at 37°C for 45 minutes prior to the assay. The optimal cell density to maintain OCR within an optimal range for both conditions was determined experimentally. Basal mitochondrial respiration was assessed by subtracting the non-mitochondrial OCR, measured with 0.5 µM antimycin A and 0.5 µM piericidin A, from baseline OCR. Coupled respiration was determined by subtracting the OCR in the presence of 1.5 µM oligomycin A (Sigma) from the basal mitochondrial respiration. Maximal respiration was determined by subtracting the OCR in the presence of 1 µM FCCP (Sigma), from baseline OCR. The XF Glycolytic Rate Assay Kit was employed to measure basal and compensatory glycolysis. Basal measurements of extracellular acidification rate (ECAR) were followed by the sequential injection of 0.5 µM rotenone/antimycin A and 50 mM 2-DG. This allowed for the calculation of the glycolytic proton efflux rate (glycoPER), representing both basal glycolysis (in the absence of mitochondrial CO_2 contribution) and compensatory glycolysis (as a result of electron transport chain inhibition). OCR and glycoPER values were normalized to 2×10^4 cells to facilitate comparison across conditions. Data analysis was performed using the Seahorse Wave desktop software.

Cancer cell transplantation

Senescence was induced as described above. To ensure there was no leakiness of Tag expression in the absence of dox, luminescence imaging was performed *in vitro*. Cancer cells were harvested by adding 0,05% trypsin (Gibco). After washing, the cells were resuspended in phosphate buffered saline (PBS) and mixed with BD Matrigel to a final concentration of 10 mg/ml. The cell suspension was kept on ice until inoculation into mice. Proliferating or senescent cancer cells were inoculated subcutaneously (s.c.) into the flanks of the mice using a 27-gauge needle (Braun). The number of cells inoculated were either 1 x 10^4 or 1 x 10^5, as specified in the figure descriptions.

Animal experiments

All animal experiments were performed according to national guidelines and were approved by the responsible national institute (Landesamt für Gesundheit und Soziales, Berlin, Germany). All mouse strains were housed at the animal facility of the Max-Delbrück Center for Molecular Medicine under specific pathogen-free conditions. For oncogene activation, doxycycline (1 mg/ml, Sigma) was administered in light-protected drinking water supplemented with 5% sucrose. To verify TagLuc expression, *in vivo* bioluminescent imaging (BLI) was performed as described previously.[17] For senolytic therapy, the weight of the mice was determined first. Lys05 (Hölzel Diagnostika) was prepared in a PBS/DMSO (25:1) solution and stored at -20°C. The drug was administered via intraperitoneal injection at a final concentration of 20 mg/kg body weight. PBS/DMSO (25:1) solution was used as a

placebo control. Tumor volumes were measured along three orthogonal axes (x, y, and z) using a caliper and calculated according to the formula V = (x*y*z)/2.

Detection of antigen-specific T cells in the blood

Detection of Tag-specific TCR expression on peripheral blood T cells was achieved by incubation with MHC/peptide tetramers and specific monoclonal antibodies in 50 µl PBS for 15 to 30 min at 4°C. The following antibodies and tetramers were used: monoclonal anti-mouse CD3ε (1:100, clone 145-2C11, Biolegend); monoclonal anti-mouse CD8a (1:100, clone 53−6.7, Biolegend); H-2Db/SAINNYAQKL (Tag peptide I) tetramer (1:100, Biozol/MBL), H-2Kb/ VVYDFLKL (Tag peptide IV) tetramer (1:1000, Biozol/MBL). Cells were washed once with PBS and resolved in 200 µl PBS before analysis using a FACS Canto II device (BD). Erythrocyte lysis was performed with BD lysing solution prior to FACS measurement. BD lysing solution was added for 8 to 10 min followed by one wash with PBS. Data was analyzed with FlowJo software (Treestar, Ashland, Oregon, USA).

Spectral Karyotyping (SKY)

Spectral Karyotyping was performed as previously described.[47] In brief, metaphase preparation was performed by treating the cells with colcemid for 60 min at a concentration of 0.035 µg/ml. Next, cells were incubated in 75 mM KCl for 20 minutes at 37°C and fixed in a freshly prepared mixture of methanol/acetic acid (3:1) at room temperature. Cell suspension was dropped onto glass slides and SKY images of 8-10 randomly selected metaphase chromosomes per cell line were acquired by staining with a mixture of 5 fluorochromes. Images were captured using an DMRXA epifluorescence microscope (Leica GmbH, Wetzlar, Germany), HCX PL SAPO 63×/1.30 oil objective (Leica), SpectraCube system (Applied Spectral Imaging, Migdal HaEmek, Israel) and analyzed using SKYView imaging software (Applied Spectral Imaging).

Apoptosis staining

Proliferating (TagLuc expressing, +dox) and senescent (TagLuc non-expressing, -dox) cells were treated with Lys05 at 5, 10 and 20 µM concentration for 7 hours at 37°C. Staining was performed with the apoptosis detection kit (Abcam) according to the manufacturer's instructions. Briefly, cells were harvested and washed twice with PBS. Next, cells were resuspended in 100 µl binding buffer solution and stained with Annexin V DY-634 and propidium iodide for 15 minutes in the dark. After incubation, 400 µl of binding buffer solution was added and analyzed via flow cytometry (BD FACS Canto II). Data was analyzed with FlowJo™ v10.8 Software (BD Life Sciences). Additionally, apoptosis was determined on the single cell level by measuring the DNA content of individual cells by flow cytometry. Cellular DNA content was measured with a logarithmic amplification in the FL-2 channel of a FACScan flow cytometer (Becton Dickinson; Heidelberg, Germany) equipped with the CellQuest software. Data are given in percent hypoploidy (i.e. the percentage of cells with a sub-G1 DNA content), which reflects the percentage of apoptotic cells with fragmented genomic DNA. Cells were collected by centrifugation at 2500 rpm, 4°C for 5 min, washed with PBS at 4°C, and fixed in PBS / 2 % (vol/vol) formaldehyde on ice for 30 min, incubated with ethanol/PBS (2 : 1, v/v) for 15 min, pelleted and resuspended in PBS containing 40 µg/ml RNase A (Roth; Karlsruhe, Germany). RNA was digested for 30 min at 37°C. Cells were pelleted again and finally resuspended in PBS containing 50 µg/ml PI (Sigma-Aldrich; Taufkirchen, Germany).

Lentiviral Production and transduction
Packaging plasmids (pMDLg/pRRE, pRSV-rev, pMD2-VSVG) and the plasmid containing the non-silencing shRNA sequence, beclin-1 TRCN 0000087288, and TRCN0000087289 pLKO.1 vectors, were transfected into Plat E-cells using Lipofectamine transfection reagent according to the manufacturer's protocol. The medium was changed 18 hours after transfection, and the supernatant was collected, filtered, and supplemented with 8 µL/mL polybrene after 24 hours. TetTagLuc#93 cells were incubated for transduction with the virus-containing medium and polybrene for 24 hours. Stable knockdown cell lines were generated by puromycin (Sigma) selection for 2–3 days following transduction.

Statistical analysis
All data were analyzed using Prism v10 (GraphPad software). Data are presented as mean ± standard deviation. Statistical analysis of the data was conducted using t-test or one-way analysis of variance (ANOVA). Data comparison with p values of ≤ 0.05 was considered statistically significant. (ns indicates not significant, $p > 0.05$; * $p \leq 0.05$; ** $p \leq 0.01$; *** $p \leq 0.001$; **** $p \leq 0.0001$)

Data Availability
The data of the mRNA sequencing, FACS and animal experiments are available upon request from the corresponding author.

ACKNOWLEDGEMENTS
We thank I. Becker, K. Borgwald and M. Pippow for technical assistance. This work was supported by a grant from the European Union (ERC Advanced Grant Neo-T, number 882963). P.S. is participant in the BIH MD Stipendium Program funded by the Charité – Universitätsmedizin Berlin and the Berlin Institute of Health at Charité (BIH). I.M.R. is supported by a Klaus Tschira Boost Fund grant from the German Scholars Organization.

AUTHOR CONTRIBUTION
P.S., I.M.R. and T.B. conceived the study, analyzed and interpreted the data and wrote the manuscript. P.S., K.H., A.M., K.A. and I.M.R. performed *in vitro* experiments. P.S. and K.H. performed tumor experiments. E.S. generated the SKY images. S.S. performed and analyzed the mRNA sequencing. B.U. performed downstream analysis and visualization of differential expression results and A.A. contributed with compute resources and supervision.

COMPETING INTEREST
The authors declare no competing interests.

REFERENCES

1. Chapman, P. B. *et al.* Improved survival with vemurafenib in melanoma with BRAF V600E mutation. *N. Engl. J. Med.* **364**, 2507–2516 (2011).
2. Hyman, D. M. *et al.* Vemurafenib in Multiple Nonmelanoma Cancers with BRAF V600 Mutations. *N. Engl. J. Med.* **373**, 726–736 (2015).
3. Roskoski, R. Small molecule inhibitors targeting the EGFR/ErbB family of protein-tyrosine kinases in human cancers. *Pharmacol. Res.* **139**, 395–411 (2019).
4. Zhao, Y. *et al.* Diverse alterations associated with resistance to KRAS(G12C)

inhibition. *Nature* **599**, 679–683 (2021).
5. Herranz, N. & Gil, J. Mechanisms and functions of cellular senescence. *J. Clin. Invest.* **128**, 1238–1246 (2018).
6. Hayflick, L. & Moorhead, P. S. The serial cultivation of human diploid cell strains. *Exp. Cell Res.* **25**, 585–621 (1961).
7. Coppé, J.-P., Desprez, P.-Y., Krtolica, A. & Campisi, J. The Senescence-Associated Secretory Phenotype: The Dark Side of Tumor Suppression. *Annu. Rev. Pathol.* **5**, 99–118 (2010).
8. Baker, D. J. *et al.* Clearance of p16Ink4a-positive senescent cells delays ageing-associated disorders. *Nature* **479**, 232–236 (2011).
9. Baker, D. J. *et al.* Naturally occurring p16(Ink4a)-positive cells shorten healthy lifespan. *Nature* **530**, 184–189 (2016).
10. Saleh, T. *et al.* Therapy-Induced Senescence: An 'Old' Friend Becomes the Enemy. *Cancers* **12**, E822 (2020).
11. Demaria, M. *et al.* Cellular Senescence Promotes Adverse Effects of Chemotherapy and Cancer Relapse. *Cancer Discov.* **7**, 165–176 (2017).
12. Coppé, J.-P. *et al.* Senescence-Associated Secretory Phenotypes Reveal Cell-Nonautonomous Functions of Oncogenic RAS and the p53 Tumor Suppressor. *PLoS Biol.* **6**, e301 (2008).
13. Krtolica, A., Parrinello, S., Lockett, S., Desprez, P. Y. & Campisi, J. Senescent fibroblasts promote epithelial cell growth and tumorigenesis: a link between cancer and aging. *Proc. Natl. Acad. Sci. U. S. A.* **98**, 12072–12077 (2001).
14. Saleh, T. *et al.* Tumor cell escape from therapy-induced senescence. *Biochem. Pharmacol.* **162**, 202–212 (2019).
15. Milanovic, M. *et al.* Senescence-associated reprogramming promotes cancer stemness. *Nature* **553**, 96–100 (2018).
16. Dörr, J. R. *et al.* Synthetic lethal metabolic targeting of cellular senescence in cancer therapy. *Nature* **501**, 421–425 (2013).
17. Anders, K. *et al.* Oncogene-targeting T cells reject large tumors while oncogene inactivation selects escape variants in mouse models of cancer. *Cancer Cell* **20**, 755–767 (2011).
18. Anders, K., Kershaw, O., Larue, L., Gruber, A. D. & Blankenstein, T. The immune system prevents recurrence of transplanted but not autochthonous antigenic tumors after oncogene inactivation therapy. *Int. J. Cancer* **141**, 2551–2561 (2017).
19. Carnero, A. Markers of Cellular Senescence. in *Cell Senescence: Methods and Protocols* (eds. Galluzzi, L., Vitale, I., Kepp, O. & Kroemer, G.) 63–81 (Humana Press, Totowa, NJ, 2013). doi:10.1007/978-1-62703-239-1_4.
20. Hara, E. *et al.* Regulation of p16CDKN2 expression and its implications for cell immortalization and senescence. *Mol. Cell. Biol.* **16**, 859–867 (1996).
21. Maciel-Barón, L. A. *et al.* Senescence associated secretory phenotype profile from primary lung mice fibroblasts depends on the senescence induction stimuli. *Age* **38**, 26 (2016).
22. Basisty, N. *et al.* A proteomic atlas of senescence-associated secretomes for aging biomarker development. *PLoS Biol.* **18**, e3000599 (2020).
23. Yuan, H. *et al.* CancerSEA: a cancer single-cell state atlas. *Nucleic Acids Res.* **47**, D900–D908 (2019).
24. Sun, D. *et al.* Discovery of AMG 232, a potent, selective, and orally bioavailable MDM2-p53 inhibitor in clinical development. *J. Med. Chem.* **57**, 1454–1472 (2014).
25. Romanov, S. R. *et al.* Normal human mammary epithelial cells spontaneously escape senescence and acquire genomic changes. *Nature* **409**, 633–637 (2001).

26. Wang, Q. *et al.* Polyploidy road to therapy-induced cellular senescence and escape. *Int. J. Cancer* **132**, 1505–1515 (2013).
27. Prasanna, P. G. *et al.* Therapy-Induced Senescence: Opportunities to Improve Anticancer Therapy. *JNCI J. Natl. Cancer Inst.* **113**, 1285–1298 (2021).
28. McAfee, Q. *et al.* Autophagy inhibitor Lys05 has single-agent antitumor activity and reproduces the phenotype of a genetic autophagy deficiency. *Proc. Natl. Acad. Sci. U. S. A.* **109**, 8253–8258 (2012).
29. Farr, J. N. *et al.* Targeting cellular senescence prevents age-related bone loss in mice. *Nat. Med.* **23**, 1072–1079 (2017).
30. Kirkland, J. L. & Tchkonia, T. Senolytic drugs: from discovery to translation. *J. Intern. Med.* **288**, 518–536 (2020).
31. Wu, C.-H. *et al.* Cellular senescence is an important mechanism of tumor regression upon c-Myc inactivation. *Proc. Natl. Acad. Sci.* **104**, 13028–13033 (2007).
32. Haferkamp, S. *et al.* Vemurafenib Induces Senescence Features in Melanoma Cells. *J. Invest. Dermatol.* **133**, 1601–1609 (2013).
33. McDermott, M. S. J. *et al.* HER2-Targeted Tyrosine Kinase Inhibitors Cause Therapy-Induced-Senescence in Breast Cancer Cells. *Cancers* **11**, 197 (2019).
34. Bojko, A. *et al.* Improved Autophagic Flux in Escapers from Doxorubicin-Induced Senescence/Polyploidy of Breast Cancer Cells. *Int. J. Mol. Sci.* **21**, E6084 (2020).
35. Mosieniak, G. *et al.* Polyploidy Formation in Doxorubicin-Treated Cancer Cells Can Favor Escape from Senescence. *Neoplasia N. Y. N* **17**, 882–893 (2015).
36. Baker, T. M., Waise, S., Tarabichi, M. & Van Loo, P. Aneuploidy and complex genomic rearrangements in cancer evolution. *Nat. Cancer* **5**, 228–239 (2024).
37. Wade, M., Li, Y.-C. & Wahl, G. M. MDM2, MDMX and p53 in oncogenesis and cancer therapy. *Nat. Rev. Cancer* **13**, 83–96 (2013).
38. Choi, P. S. *et al.* Lymphomas that recur after MYC suppression continue to exhibit oncogene addiction. *Proc. Natl. Acad. Sci. U. S. A.* **108**, 17432–17437 (2011).
39. Liu, J. & Debnath, J. The Evolving, Multifaceted Roles of Autophagy in Cancer. *Adv. Cancer Res.* **130**, 1–53 (2016).
40. Autophagy in malignant transformation and cancer progression. *EMBO J.* **34**, 856–880 (2015).
41. Was, H. *et al.* Bafilomycin A1 triggers proliferative potential of senescent cancer cells in vitro and in NOD/SCID mice. *Oncotarget* **8**, 9303–9322 (2017).
42. Aqbi, H. F. *et al.* Autophagy-deficient breast cancer shows early tumor recurrence and escape from dormancy. *Oncotarget* **9**, 22113–22122 (2018).
43. Love, M. I., Huber, W. & Anders, S. Moderated estimation of fold change and dispersion for RNA-seq data with DESeq2. *Genome Biol.* **15**, 550 (2014).
44. Grinat, J. *et al.* The epigenetic regulator Mll1 is required for Wnt-driven intestinal tumorigenesis and cancer stemness. *Nat. Commun.* **11**, 6422 (2020).
45. Kolberg, L., Raudvere, U., Kuzmin, I., Vilo, J. & Peterson, H. gprofiler2 -- an R package for gene list functional enrichment analysis and namespace conversion toolset g:Profiler. *F1000Research* **9**, ELIXIR-709 (2020).
46. Korotkevich, G. *et al.* Fast gene set enrichment analysis. *bioRxiv* 060012 (2021) doi:10.1101/060012.
47. Conde, M. *et al.* Chromosomal instability induced by increased BIRC5/Survivin levels affects tumorigenicity of glioma cells. *BMC Cancer* **17**, 889 (2017).

Figure Legends

Figure 1: Oncogene inactivation induces senescence and a pro-inflammatory SASP.

A, Schematic of the mouse model. The model features the SV40 large T antigen (Tag) oncogene regulated by a tetracycline response element (TRE). Addition or withdrawal of doxycycline (dox) activates or inactivates the oncogene, respectively. The Tag is fused to firefly luciferase (Luc), creating the TagLuc fusion protein, which serves as both a cancer driver and a reporter for intravital imaging. Oncogene activation and inactivation are reversible in both in vitro and in vivo settings. **B,** Western blot analysis of TagLuc in clone 4 and TTC #3055 cells cultured in the presence of dox or at different time points after dox withdrawal. β-actin was used as a loading control. MCA-205 served as negative control. A shorter splicing product of Tag (~ 100KDa), sTagLuc was detected. Shown is one representative experiment out of four independent experiments. **C,** Clone 4 and TTC #3055 cells were grown in the presence or absence of dox and live cell number was assessed at different time points. Error bars indicate standard deviation; n=2 technical replicates. **D,** BrdU incorporation following TagLuc inactivation was analyzed to determine cell cycle phase distribution. The presented data represent one representative experiment out of three conducted. **E,** Upper pictures show morphological changes of clone 4 cells growing on dox or after three- or seven-days post TagLuc inactivation detected by phase-contrast light microscopy. Black arrows indicate enlarged and flattened cells with irregular shape. Lower pictures show SA-β-galactosidase staining of clone 4 cells growing on dox or after four-or seven-days post TagLuc inactivation. Shown is one representative image out of three independent experiments. **F,** Clone 4 cells were cultured with or without dox for two weeks. Conditioned medium was generated and normalized to cell number ($2x10^5$ cells/ml). Il6 and Mmp3 secretion was analyzed via ELISA. Error bars indicate standard deviation. Il6: n = 4, pooled data from two independent experiments comprising two samples, ** $p < 0,01$. Mmp3: n = 2 technical replicates from one experiment, * $p < 0,05$.

Extended Data Figure 1. Characterization of senescence and SASP profiles following oncogene inactivation

A, Luciferase reporter activity in the presence of dox or at different time points following dox deprivation in clone 4 and TTC #3055 cells. Exposure time: 1s. Error bars indicate standard deviation; n=3 independent experiments. MCA-205 cells serve as negative control. **B,** The viability of clone 4 cancer cells was quantified 12 to 14 days after oncogene inactivation. The percentage of surviving clone 4 cells was calculated relative to the initial cell number before oncogene inactivation; n=19 independent experiments. **C,** Morphological changes of TTC #3055 cells were observed under phase-contrast light microscopy after growth on dox or at three- or seven-days post TagLuc inactivation. Enlarged and flattened cells with irregular shapes are indicated by black arrows. Data from one experiment are shown, although the observed phenotype was consistently observed. **D,** Levels of CDKN1A (p21) and CDKN2A (p16) mRNA relative to GAPDH mRNA in proliferating (TagLuc expressing, +dox) and senescent (TagLuc non-expressing, -dox) clone 4 cells measured by real-time PCR. Error bars indicate standard deviation; n=3 technical replicates. * $p < 0,05$, ** $p < 0,01$. **E,** Secretion of cytokines in proliferating (TagLuc expressing, +dox) and senescent (TagLuc non-expressing, -dox) cells. The experiment was conducted once. A comprehensive annotation of the array can be found in Supplementary Document 3.

Figure 2: Senescence is accompanied by major transcriptional changes and the acquisition of a plurimetabolic state.
A, B, Enriched pathway terms (KEGG/Reactome) among the downregulated (A) and upregulated (B) genes in senescent (TagLuc non-expressing, -dox) cells compared to proliferating (TagLuc expressing, +dox) cells. The complete dataset of differentially expressed genes can be found in Supplementary Document 1. n=3 technical replicates. **C, D,** Gene-set enrichment analysis using cancer state signature genes (CancerSEA) downregulated (C) and upregulated (D) in senescent (TagLuc non-expressing, -dox) cells compared to proliferating (TagLuc expressing, +dox) cells. n=3 technical replicates. **E. F,** Basal (E) and compensatory (F) glycolysis in senescent (TagLuc non-expressing, -dox) cells compared to proliferating (TagLuc expressing, +dox) cells. Data are mean ± s.e.m; n = 3 independent experiments. *$p < 0.05$, two-tailed t-tests. **G, H, I,** Basal (G), coupled (H) and maximal (I) respiration in senescent (TagLuc non-expressing, -dox) cells compared to proliferating (TagLuc expressing, +dox) cells. Data are mean ± s.e.m; n = 3 independent experiments. *$p < 0.05$, two-tailed t-tests.

Extended Data Figure 2: Transcriptional and metabolic changes in senescent *versus* proliferating cancer cells.
A, Volcano plot showing the differentially upregulated and downregulated genes in senescent (TagLuc non-expressing, -dox) cells compared to proliferating (TagLuc expressing, +dox) cells. **B,** Differential expression of genes associated with SASP in senescent (TagLuc non-expressing, -dox) cells compared to proliferating (TagLuc expressing, +dox) cells. **C, D,** p-values derived from GSEA of cancer state signature genes (CancerSEA) downregulated (C) and upregulated (D) in senescent (TagLuc non-expressing, -dox) cells compared to proliferating (TagLuc expressing, +dox) cells. **E,** Representative profile of the extra-cellular acidification rate after addition of the complex I (rotenone) and complex III (antimycin) inhibitors and the glycolytic inhibitor (2-DG). **F,** Representative profile of the oxygen consumption rate after addition of the complex V inhibitor (oligomycin), the uncoupler (FCCP), and the complex I inhibitor (rotenone) and complex III inhibitor (antimycin) in proliferating (TagLuc expressing, +dox) and senescent (TagLuc non-expressing, -dox) cells.

Figure 3: The acquisition of a senescent state facilitates cancer relapse.
A, Schematic representation of the mouse cancer model. Cancer cells growing in the absence of dox for 14 days were subcutaneously injected into CM2 mice. After 4 weeks, TagLuc was activated by providing dox through the drinking water. Marked in grey is the occurrence of tumor relapse following initial tumor rejection. **B,** Representative immunocompetent (rtTA expressing, CM2) mouse subcutaneously inoculated with senescent (TagLuc non-expressing, -dox) clone 4 cells. TagLuc expression was re-induced after 4 weeks of a resting time by dox administration (200 µg/ml). TagLuc signal was measured by BL imaging (exposure time: 60 s) and followed over time. **C,** Bioluminescence signal kinetics over time are displayed for immunodeficient (Rag2-KO, n=6) and immunocompetent (CM2, n=7) mice inoculated with senescent (TagLuc non-expressing, -dox) clone 4 cells. Data are from two independent experiments. **D,** Tumor outgrowth in immunodeficient (Rag2-KO, n=6) mice and relapse tumor growth in immunocompetent (CM2, n=10) mice following tumor rejection of clone 4 cells. Data are from three independent experiments. Note: one mouse died before relapse could be assessed. **E,** Bioluminescence signal kinetics over time are displayed for immunodeficient (Rag2-KO, n=5) and immunocompetent (CM2, n=6) mice inoculated with senescent (TagLuc non-

expressing, -dox) TTC #3055 cells. Data from one experiment. **F,** Tumor outgrowth in immunodeficient (Rag2-KO, n=5) mice and relapse tumor growth in immunocompetent (CM2, n=6) mice following tumor rejection of TTC #3055 cells. Data from one experiment. Note: two mice died before relapse could be assessed. **G,** Relapse frequency in experimental conditions where proliferating (TagLuc expressing, +dox), or senescent (TagLuc non-expressing, -dox) clone 4 or TTC #3055 were inoculated. **H,** Schematic representation of the mouse cancer model with persistent senescence. $1x10^4$ senescent, TagLuc non-expressing clone 4 cells (marked in blue) were subcutaneously injected into CM2 mice, which remained off dox throughout the experimental period. Although the oncogene was never activated, Tag-independent tumors (marked in grey) grew out in 10 out of 12 cases. **I,** Growth kinetics of tumors with permanent TagLuc inactivation; n = 12 from two independent experiments.

Extended Data Figure 3. TagLuc independent growth of relapsed tumors.
A, Clone 4 cells were cultured in the presence of doxycycline (dox). Subsequently, $1x10^4$ TagLuc proliferating (TagLuc expressing, +dox) clone 4 cells were subcutaneously injected into immunocompetent (CM2) mice. Mice were continuously provided with dox-supplemented drinking water to maintain oncogene activation. **B,** Representative mouse inoculated with proliferating clone 4 cells. TagLuc signal was measured by BL imaging (exposure time: 60 s) and followed over time. **C,** Bioluminiscence signal kinetics over time in immunodeficient (Rag2-KO, n=4) and immunocompetent (CM2, n=5) mice inoculated with proliferating (TagLuc expressing, +dox) clone 4 cells. Data from one experiment. **D**, **E,** Percentage of Tag-specific T cells in the blood of immunized C57BL/6 or tumor bearing CM2 mice, 10 days after tumor cell injections (D) or at different time points after oncogene re-activation (E). Naïve mice served as control. Representative dot blots are shown. **F,** Relative light units (RLU) per µg protein for parental clone 4 cells and cancer cell lines from relapsed tumors, cultured both with and without dox. Four out of five relapse cell lines showed no significant TagLuc activity in the presence of dox, and no light signal was detected in the absence of dox. Error bars indicate standard deviation; n = 2 technical replicates, ns = not significant, **** $p < 0,0001$. **G,** mRNA sequencing analysis was conducted on parental and relapsed cancer cell lines to compare the expression levels of Tag. The figure shows the normalized read counts for each sample; n=3 technical replicates.

Figure 4: Cancer cells re-isolated from relapsed tumors depend on Mdm2 and acquired poliploidy.
A, mRNA sequencing of the parental (+dox and -dox) clone 4 cells and relapsed cancer cell lines was performed. The number of differentially upregulated and downregulated genes between the parental (+dox and -dox) clone 4 cells and the relapsed cancer cells is shown in the Venn diagram. **B,** The graph shows the genes that are upregulated and downregulated in relapsed cancer cell lines compared to proliferating (TagLuc expressing, +dox) and senescent (TagLuc non-expressing, -dox) clone 4 cells. Genes highlighted in “red” are the top 10 genes that show the most drastic average log2-fold-changes in both comparisons in either direction (positive/negative). Genes highlighted in “blue” are also relevantly up- or downregulated genes and had been preselected as potential candidates of targeted therapy. **C,** Relative cell growth of parental clone 4 cells and cancer cell lines from relapsed tumors (#677, #680) following treatment with the Mdm2 inhibitor AMG 232 (1 µM for 72 hours). Cell growth was calculated by comparing the cell number after

treatment to the initial cell number. Error bars indicate standard deviation; n=3 independent experiments, ns = not significant, **** p < 0,0001. **D, E, F,** Spectral karyotyping (SKY) images of parental proliferating Clone 4 cells expressing TagLuc (+dox) (D), a re-isolated cancer cell line from a relapsed tumor after transient TagLuc inactivation (E), and a re-isolated cancer cell line from a tumor that emerged following persistent TagLuc inactivation (F). SKY images were obtained from 8-10 randomly selected metaphase chromosomes per cell line, with one representative example shown. Supplementary Document 5 details the chromosomal aberrations observed in the 10 selected metaphase chromosomes of the parental Clone 4 cells.

Extended Data Figure 4: Relapsed tumors are transcriptionally distinct from parental proliferating and senescent cells.
A, B, Top enriched terms/pathways detected among upregulated (A) and downregulated (B) genes in relapsed cancer cell lines compared to parental (+dox and -dox) clone 4 cells. **C,** The distribution of different chromosomes, along with the number of copies of each chromosome in each cell, was examined in the parental clone 4 cells expressing TagLuc. **D,** Spectral karyotyping of a cancer cell line re-isolated from a relapsed tumor after transience senescence. SKY images of 8-10 randomly selected metaphase chromosomes per cell line were acquired. Shown is one additional representative example.

Figure 5: Autophagy-targeted therapy has senolytic effects *in vitro* but is unable to prevent cancer relapse.
A, Proliferating (TagLuc expressing, +dox) and senescent (TagLuc non-expressing, -dox) cells were treated with Lys05 at the indicated concentration for 7 hours and subsequently stained with Annexin V and propidium iodide (PI). The distribution of live (Annexin V-/PI-), apoptotic (Annexin V+/PI-), and dead cells (Annexin V+/PI+) is shown. Error bars indicate standard deviation; pooled data from three independent experiments, each experiment comprising one sample. **B,** Tet-TagLuc cells were cultured in the absence (day 0) or presence of dox as indicated. Western blot analysis of Beclin-1, LC3-I and LC3-II in non-targeting shRNA control and shRNA Beclin1-1 Tet-TagLuc cells. Actin was used as a loading control. **C,** DNA fragmentation analysis of non-targeting shRNA control and shRNA targeting Beclin-1_1 Tet-TagLuc cells cultured in the absence or presence of dox as indicated. Shown is one representative experiment out of two independent experiments. Data are mean ± s.d; n = 2 technical replicates. * p < 0,05. **D,** Timeline of in vivo experimental conditions: cells were grown without dox for 14 days before inoculation into mice. 1 $x10^4$ senescent (TagLuc non-expressing) clone 4 cells were subcutaneously injected into CM2 mice. One week after tumor injections, mice were treated with Lys05 or placebo via intraperitoneal (i.p.) injection. Mice were monitored for 16 weeks post-cell injection and tumor volume was measured. **E,** Tumor outgrowth in immunocompetent (CM2) mice following tumor injections of senescent cells and without oncogene activation (persistent senescene). Mice were treated with 2 cycles of 3 doses of Lys05 (20 mg/kg, n=15) or placebo (PBS/DMSO, n=14). Each treatment cycle included a one-week pause between doses. **F,** Tumor volume at day 95 post tumor injections in mice treated with 2 cycles of 3 doses of Lys05 (20 mg/kg, n=15) or placebo (PBS/DMSO, n=14). Each treatment cycle included a one-week pause between doses. * p < 0,05. **G,** Timeframe of the in vivo experimental conditions: TagLuc cells were grown in the presence of dox. One week before tumor cell injections, Rag-KO mice received dox in the drinking water. TagLuc was inactivated by withdrawing dox *in vivo* on day 70. Three days post dox withdrawal, mice were

treated with Lys05 or placebo via intraperitoneal (i.p.) injection. Mice were monitored, and tumor volume was measured. **H**, Tumor outgrowth in immunodeficient (Rag-KO) mice following TagLuc inactivation and treatment with 2 cycles of 3 doses of Lys05 (20 mg/kg, n=12) or placebo (PBS/DMSO, n=12). Each treatment cycle included a one-week pause between doses. One mice treated with Lys05 died on day 77 due to non-therapy related complications. **I,** Tumor volume at day 98 post tumor injections in mice treated with 2 cycles of 3 doses of Lys05 (20 mg/kg, n=12) or placebo (PBS/DMSO, n=12) following TagLuc inactivation in stablished tumors. * $p < 0,05$.

Extended Data Figure 5. Autophagy inhibition does not affect tumor growth of proliferating cells *in vivo*.

A, The fraction of living cells after Lys05 treatment at different concentrations was normalized to the untreated population. Error bars indicate standard deviation; n = 3 independent experiments, ** $p < 0,01$, *** $p < 0,001$. **B,** Tet-TagLuc cells were cultured in the absence (day 0) or presence of dox as indicated. Western blot analysis of Beclin-1, LC3-I and LC3-II in non-targeting shRNA control and shRNA Beclin1-2 cells. Actin was used as a loading control. **C,** DNA fragmentation analysis of non-targeting shRNA control and shRNA targeting Beclin-1_2 Tet-TagLuc cells cultured in the absence or presence of dox as indicated. Shown is one representative experiment out of two independent experiments. Data are mean ± s.d; n = 2 technical replicates. * $p < 0,05$. **D,** Western blot analysis of procaspase-3 in non-targeting shRNA control and shRNA Beclin1-1 and shRNA Beclin1_2 cells. Actin was used as a loading control. **E,** Proliferating cells expressing TagLuc (+dox) were subcutaneously inoculated into immunodeficient Rag-KO mice. Dox was administered continuously to the mice throughout the experiment to ensure sustained oncogene expression. One week after tumor cell injections, mice were treated with Lys05 or placebo. **F,** Tumor outgrowth in Rag-KO mice injected with proliferating (TagLuc expressing, +dox) cells and treated with 2 cycles of 3 doses of Lys05 (20 mg/kg, n=5) or placebo (PBS/DMSO, n=5).

Figure 1.

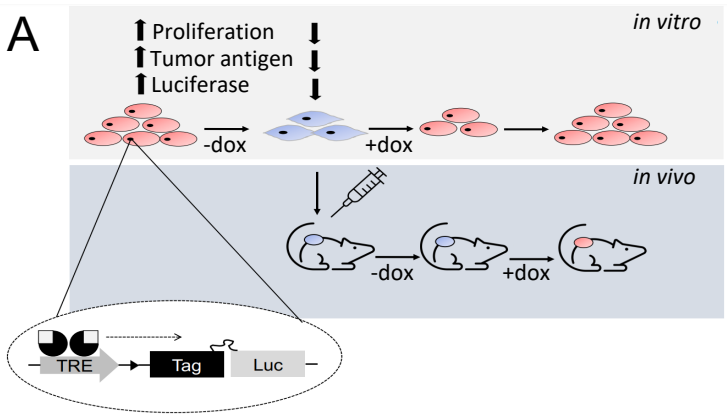
A
Proliferation
Tumor antigen
Luciferase
in vitro
-dox
+dox
in vivo
-dox
+dox
TRE
Tag
Luc

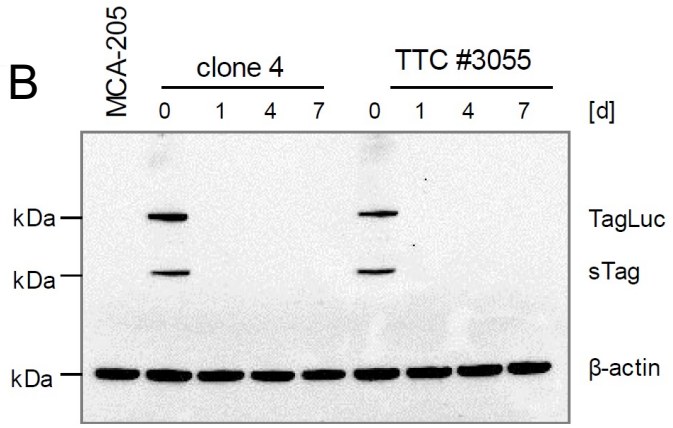
B
MCA-205
clone 4
TTC #3055
0 1 4 7 0 1 4 7 [d]
kDa
kDa
kDa
TagLuc
sTag
β-actin

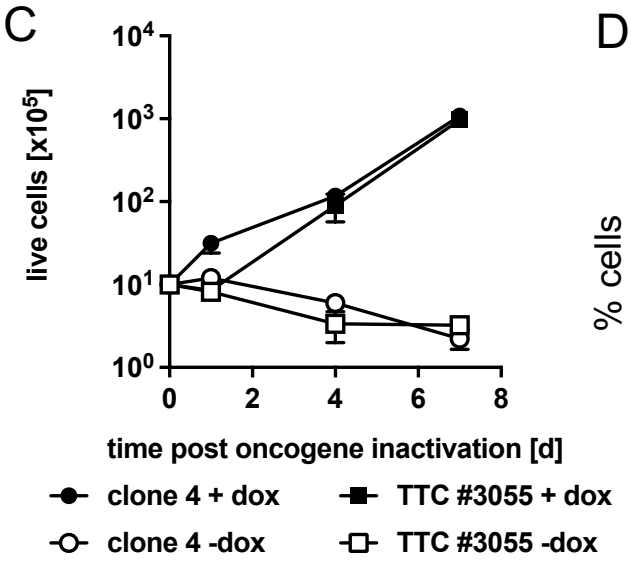
C
live cells [x10^5]
10^4
10^3
10^2
10^1
10^0
0 2 4 6 8
time post oncogene inactivation [d]
clone 4 + dox
TTC #3055 + dox
clone 4 -dox
TTC #3055 -dox

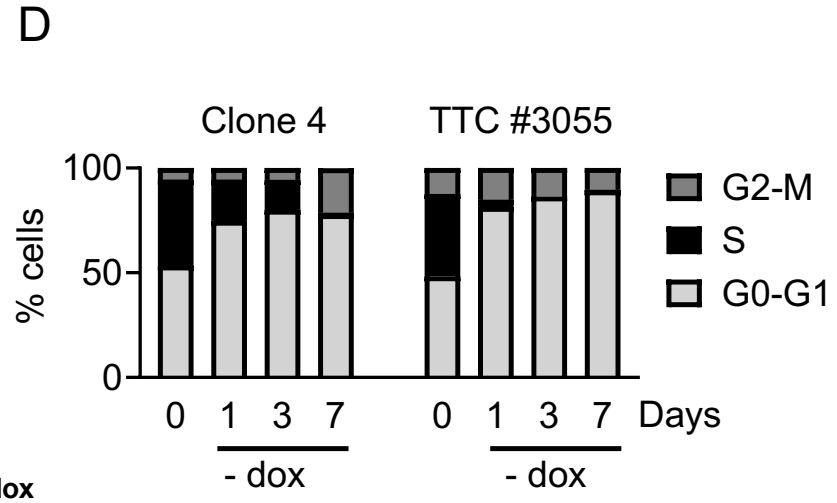
D
Clone 4
TTC #3055
% cells
100
50
0
G2-M
S
G0-G1
0 1 3 7 0 1 3 7 Days
- dox
- dox

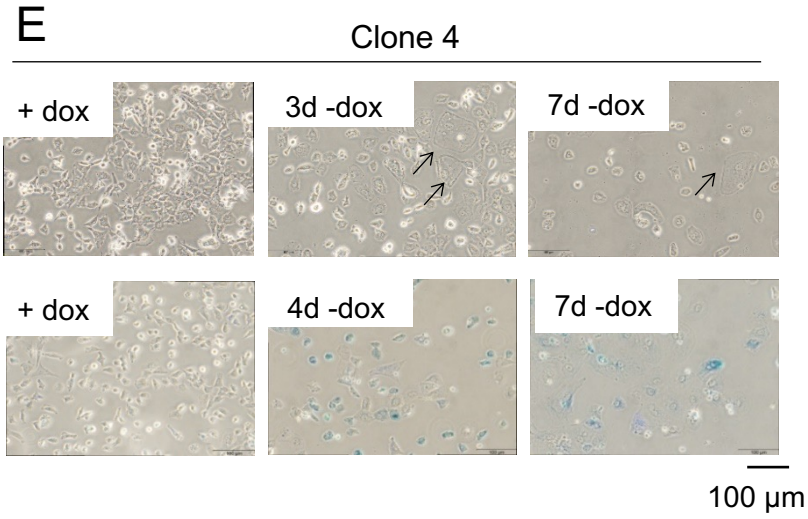
E
Clone 4
+ dox
3d -dox
7d -dox
+ dox
4d -dox
7d -dox
100 µm

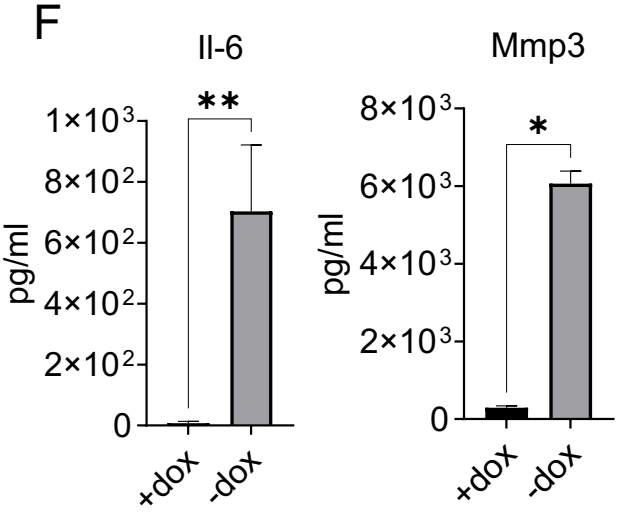
F
Il-6
Mmp3
pg/ml
1×10^3
8×10^2
6×10^2
4×10^2
2×10^2
0
**
8×10^3
6×10^3
4×10^3
2×10^3
0
*
+dox
-dox

Extended Figure 1.

A

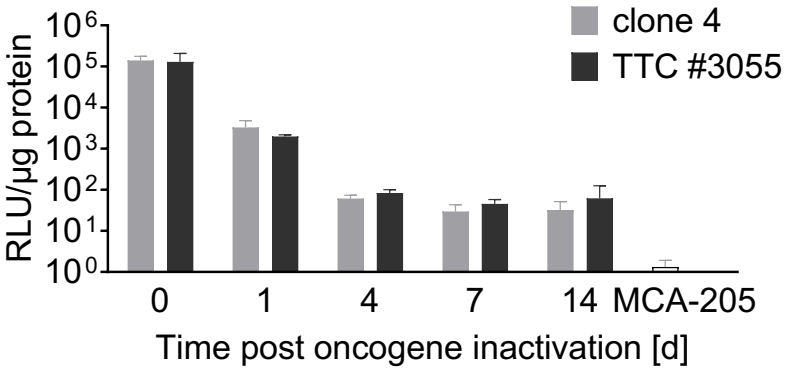

B

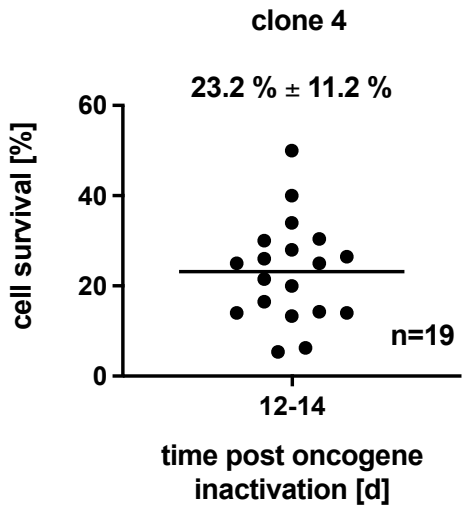

C

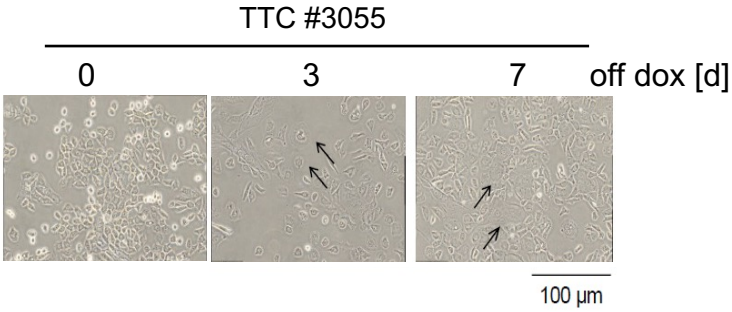

D

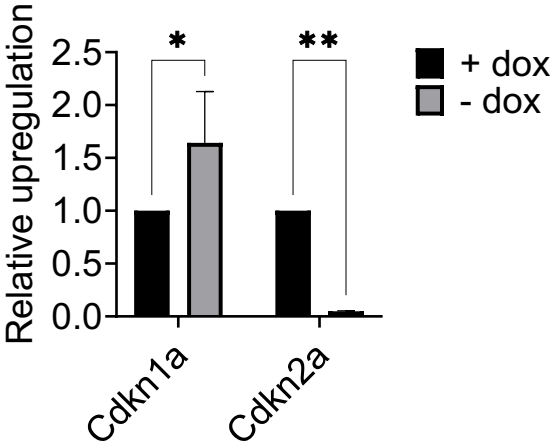

E

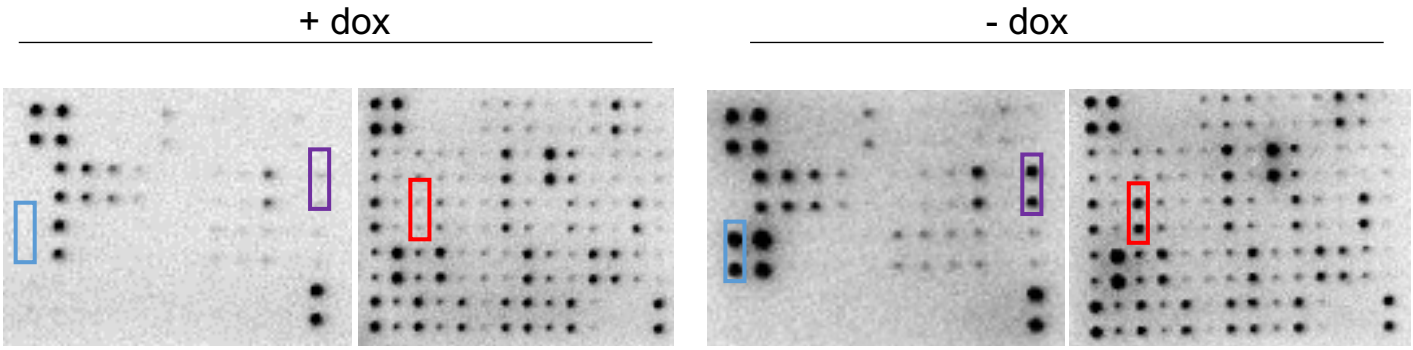

Mmp3, Mmp2, Il-6

Figure 2.

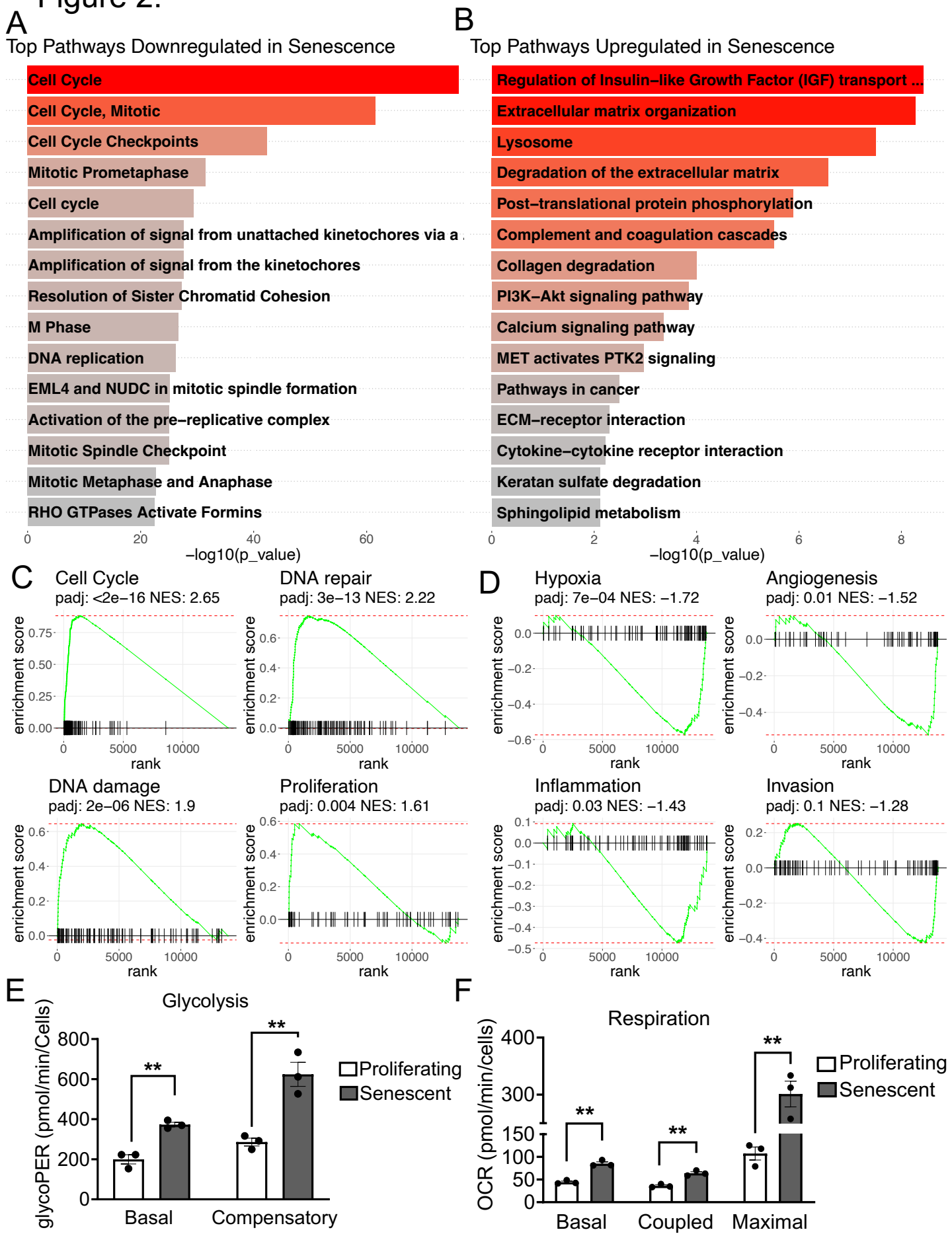
A
Top Pathways Downregulated in Senescence
Cell Cycle
Cell Cycle, Mitotic
Cell Cycle Checkpoints
Mitotic Prometaphase
Cell cycle
Amplification of signal from unattached kinetochores via a
Amplification of signal from the kinetochores
Resolution of Sister Chromatid Cohesion
M Phase
DNA replication
EML4 and NUDC in mitotic spindle formation
Activation of the pre−replicative complex
Mitotic Spindle Checkpoint
Mitotic Metaphase and Anaphase
RHO GTPases Activate Formins
0
20
40
60
−log10(p_value)
B
Top Pathways Upregulated in Senescence
Regulation of Insulin−like Growth Factor (IGF) transport ...
Extracellular matrix organization
Lysosome
Degradation of the extracellular matrix
Post−translational protein phosphorylation
Complement and coagulation cascades
Collagen degradation
PI3K−Akt signaling pathway
Calcium signaling pathway
MET activates PTK2 signaling
Pathways in cancer
ECM−receptor interaction
Cytokine−cytokine receptor interaction
Keratan sulfate degradation
Sphingolipid metabolism
0
2
4
6
8
−log10(p_value)
C
Cell Cycle
padj: <2e−16 NES: 2.65
DNA repair
padj: 3e−13 NES: 2.22
DNA damage
padj: 2e−06 NES: 1.9
Proliferation
padj: 0.004 NES: 1.61
enrichment score
rank
D
Hypoxia
padj: 7e−04 NES: −1.72
Angiogenesis
padj: 0.01 NES: −1.52
Inflammation
padj: 0.03 NES: −1.43
Invasion
padj: 0.1 NES: −1.28
enrichment score
rank
E
Glycolysis
glycoPER (pmol/min/Cells)
Basal
Compensatory
Proliferating
Senescent
**
F
Respiration
OCR (pmol/min/cells)
Basal
Coupled
Maximal
Proliferating
Senescent
**

Extended Figure 2.

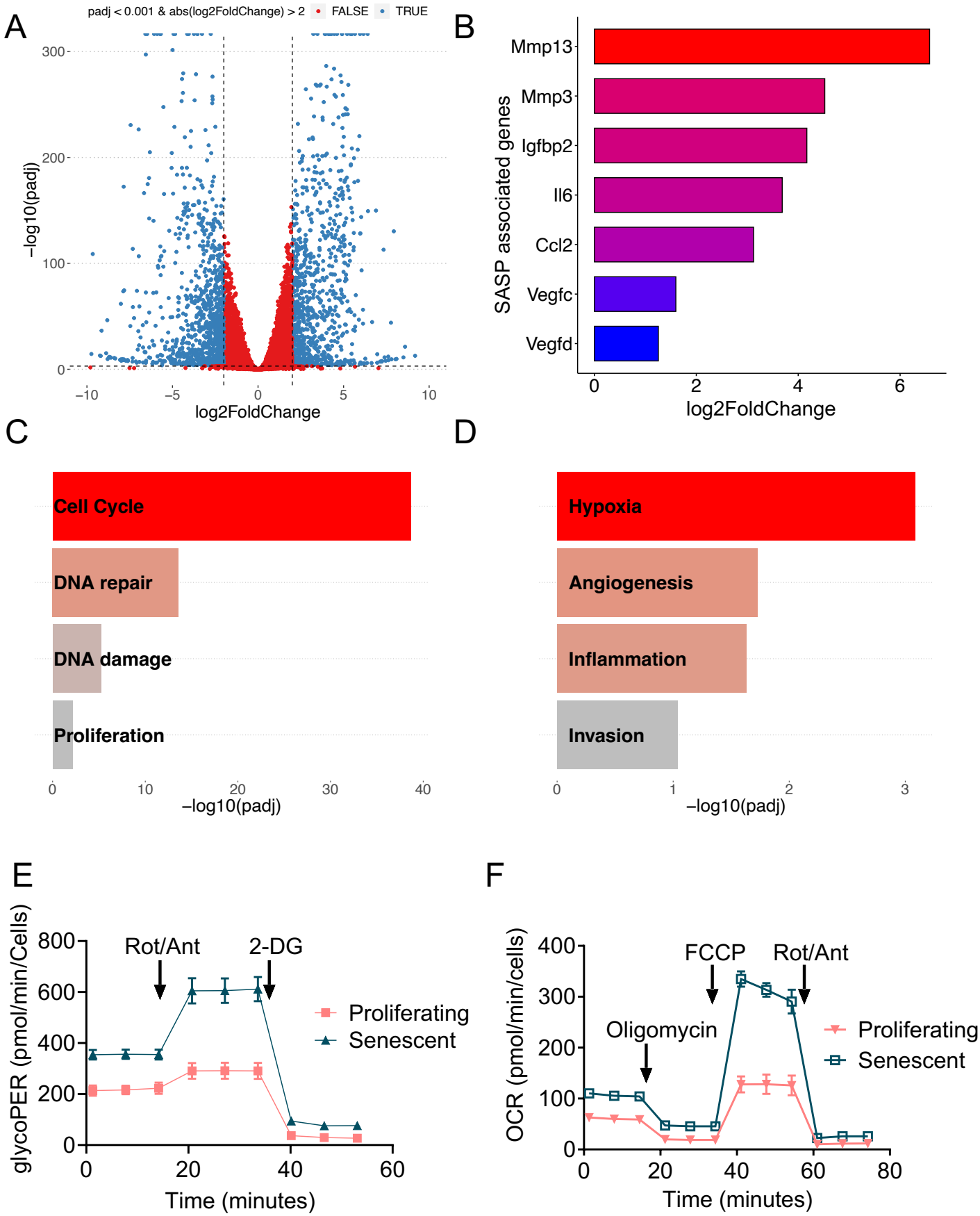

Figure 3.

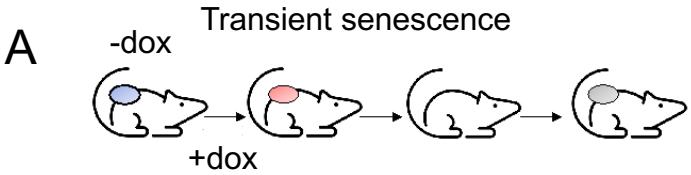

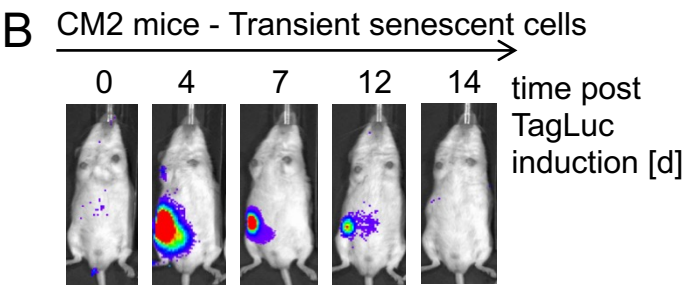

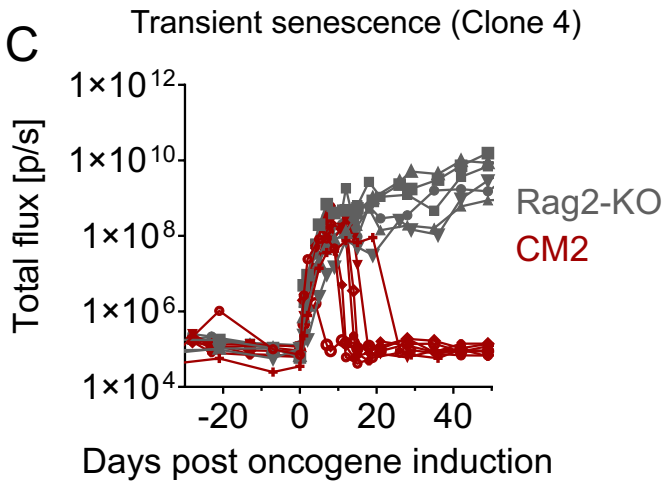

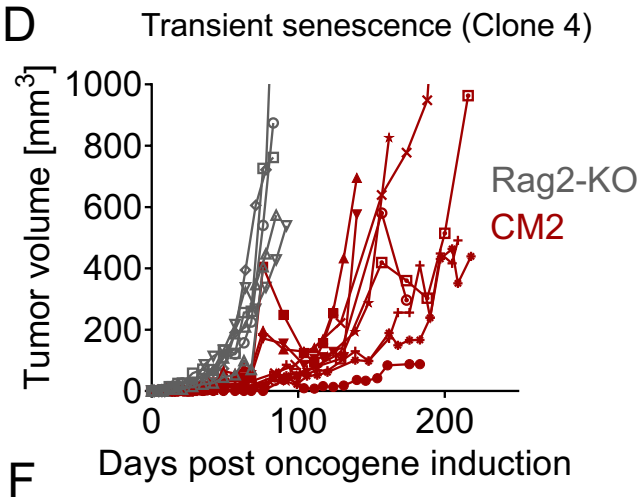

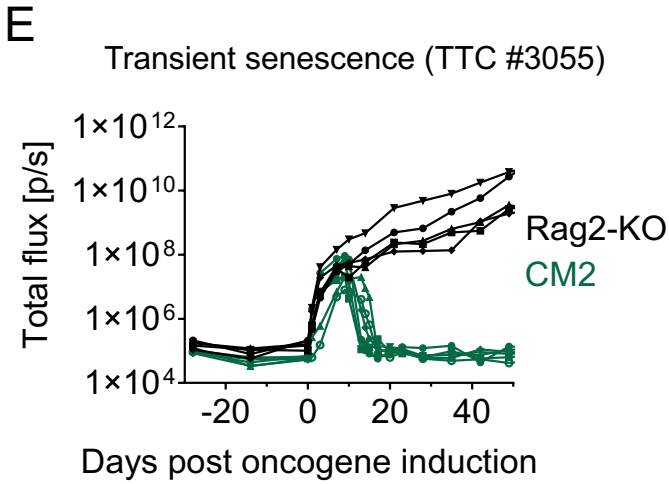

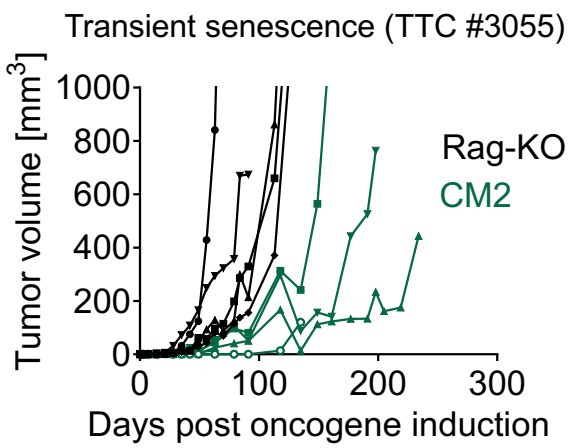

G

	Relapse frequency
Proliferating cells (Clone 4)	0/9
Transient senescence (Clone 4)	9/9
Transient senescence (TTC #3055)	4/4

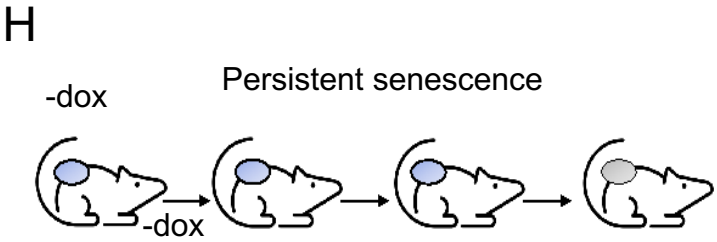

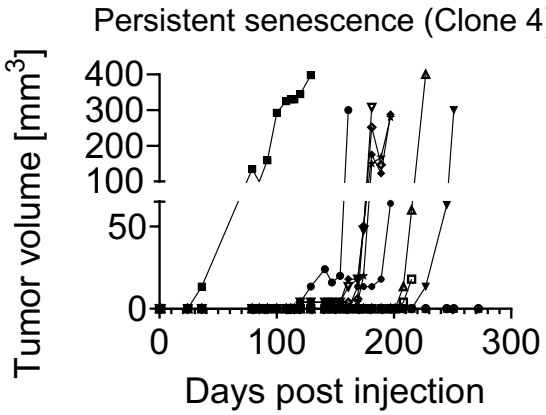

Extended Figure 3.

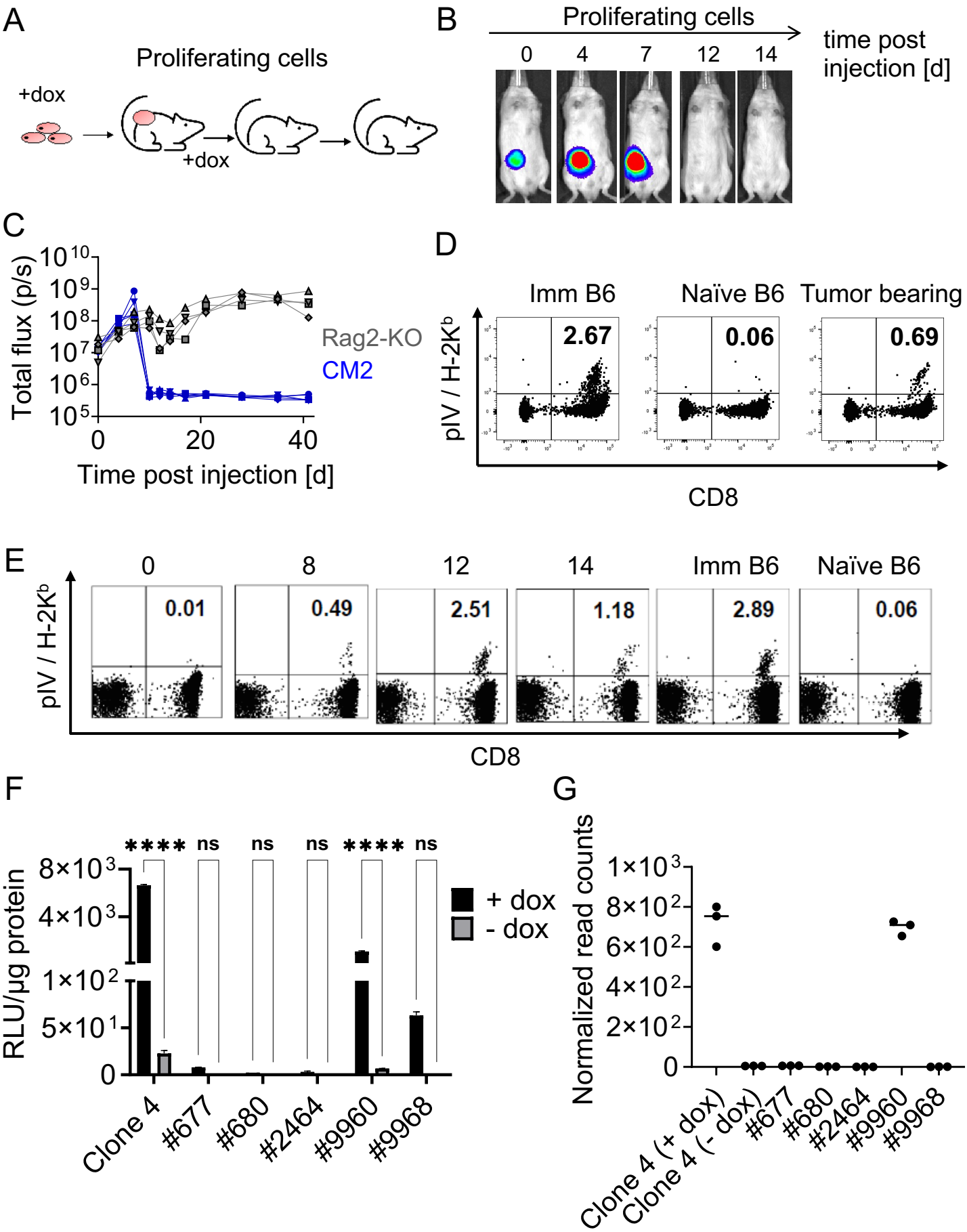

Figure 4.

A

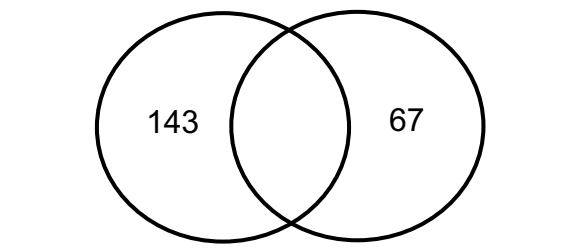

B

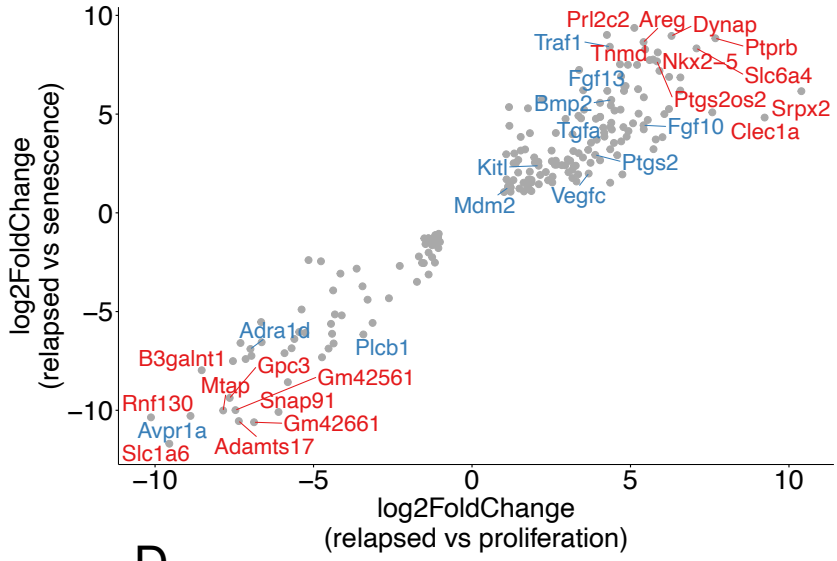

C

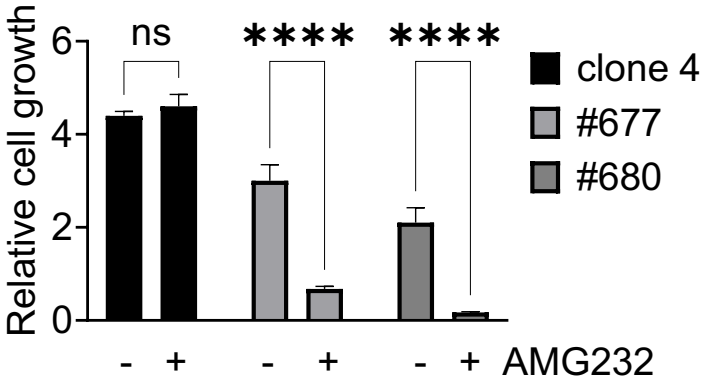

D

Parental cell line

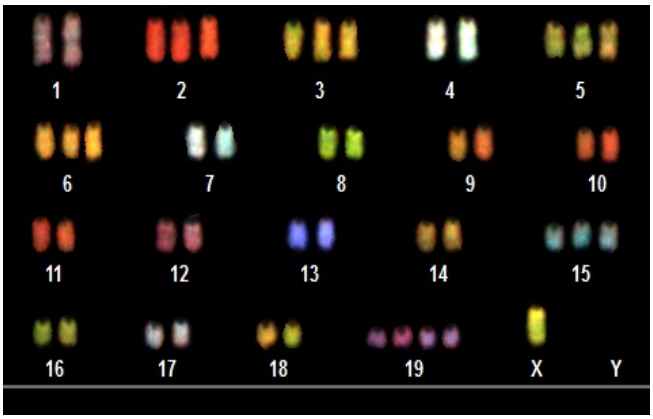

E

Transient senescence

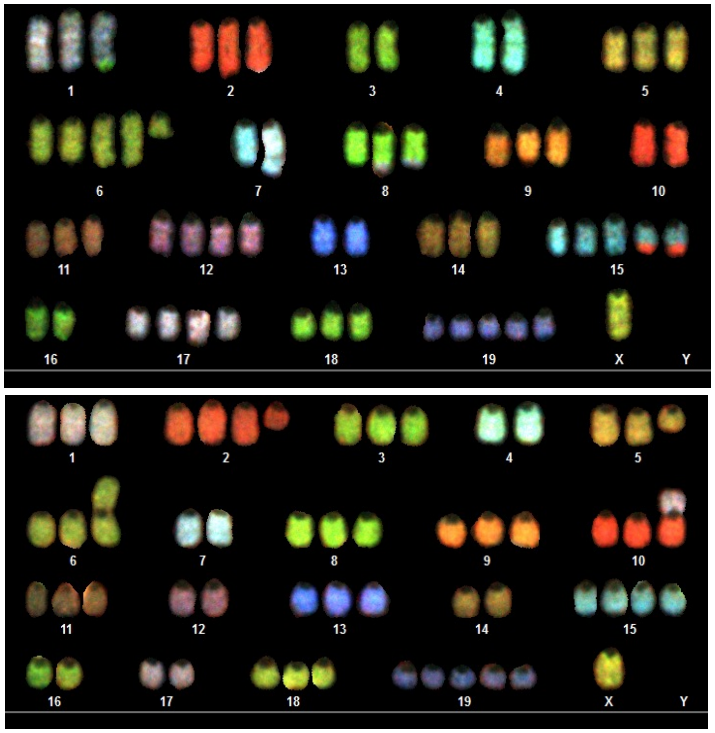

F

Persistent senescence

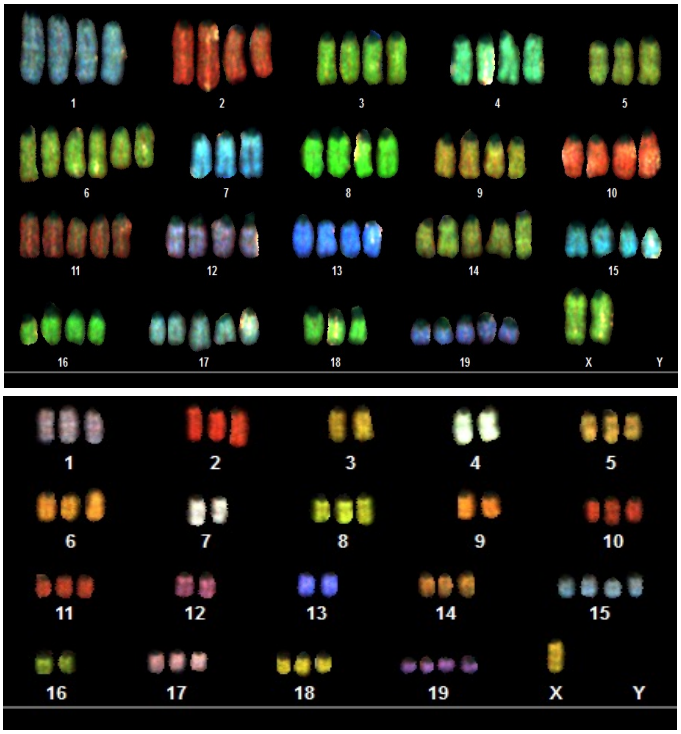

Extended Figure 4.

A

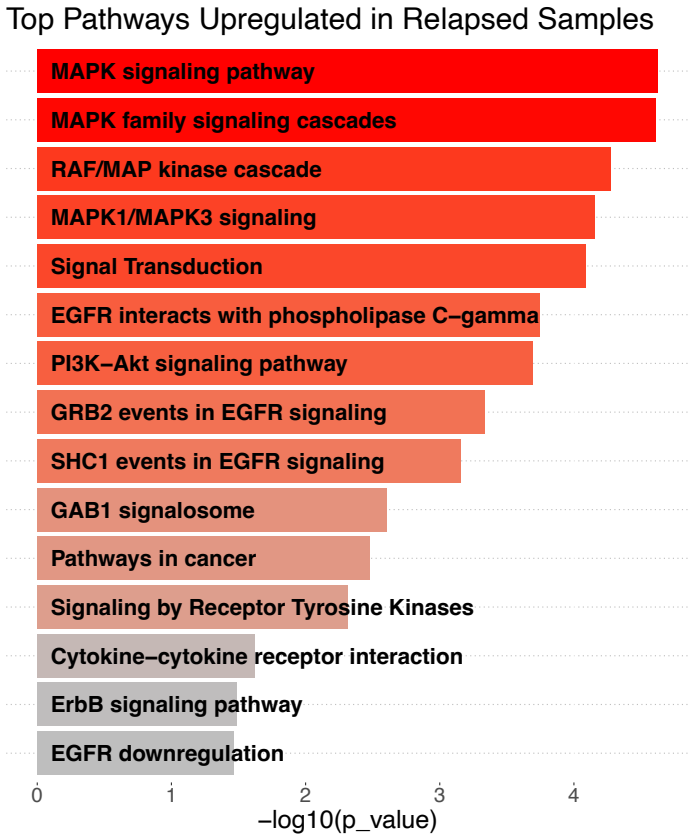

B

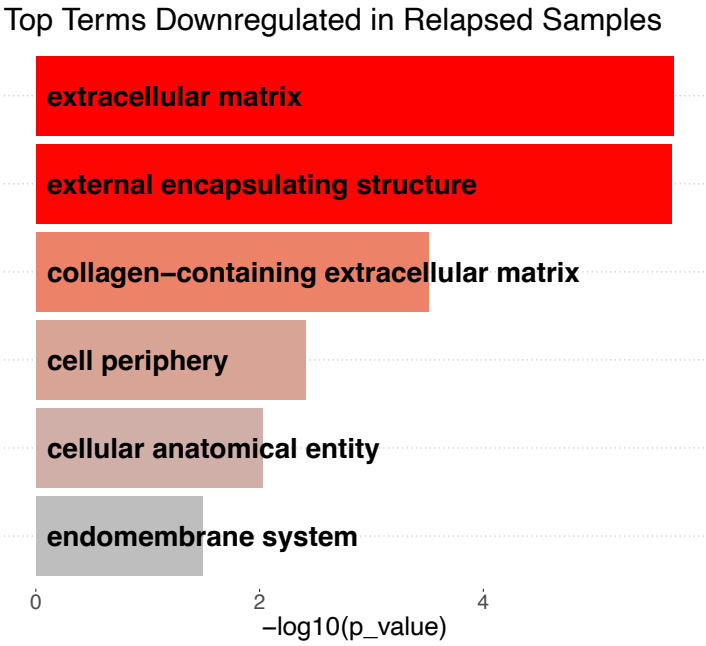

C

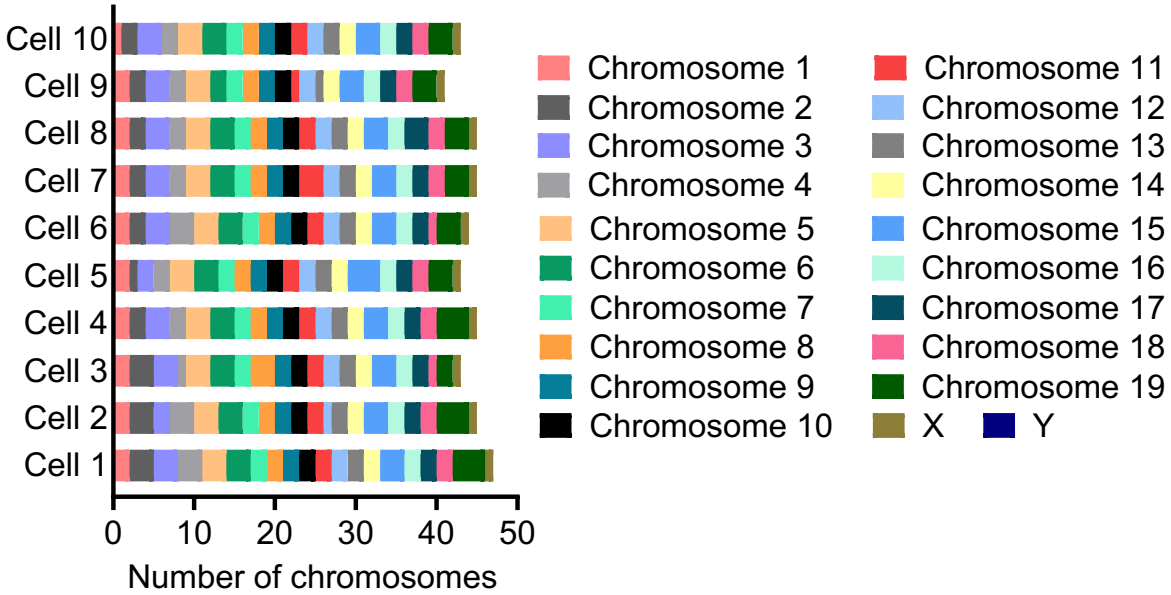

D

Transient senescence

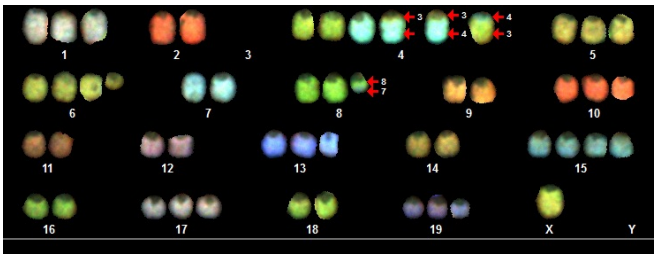

Figure 5.

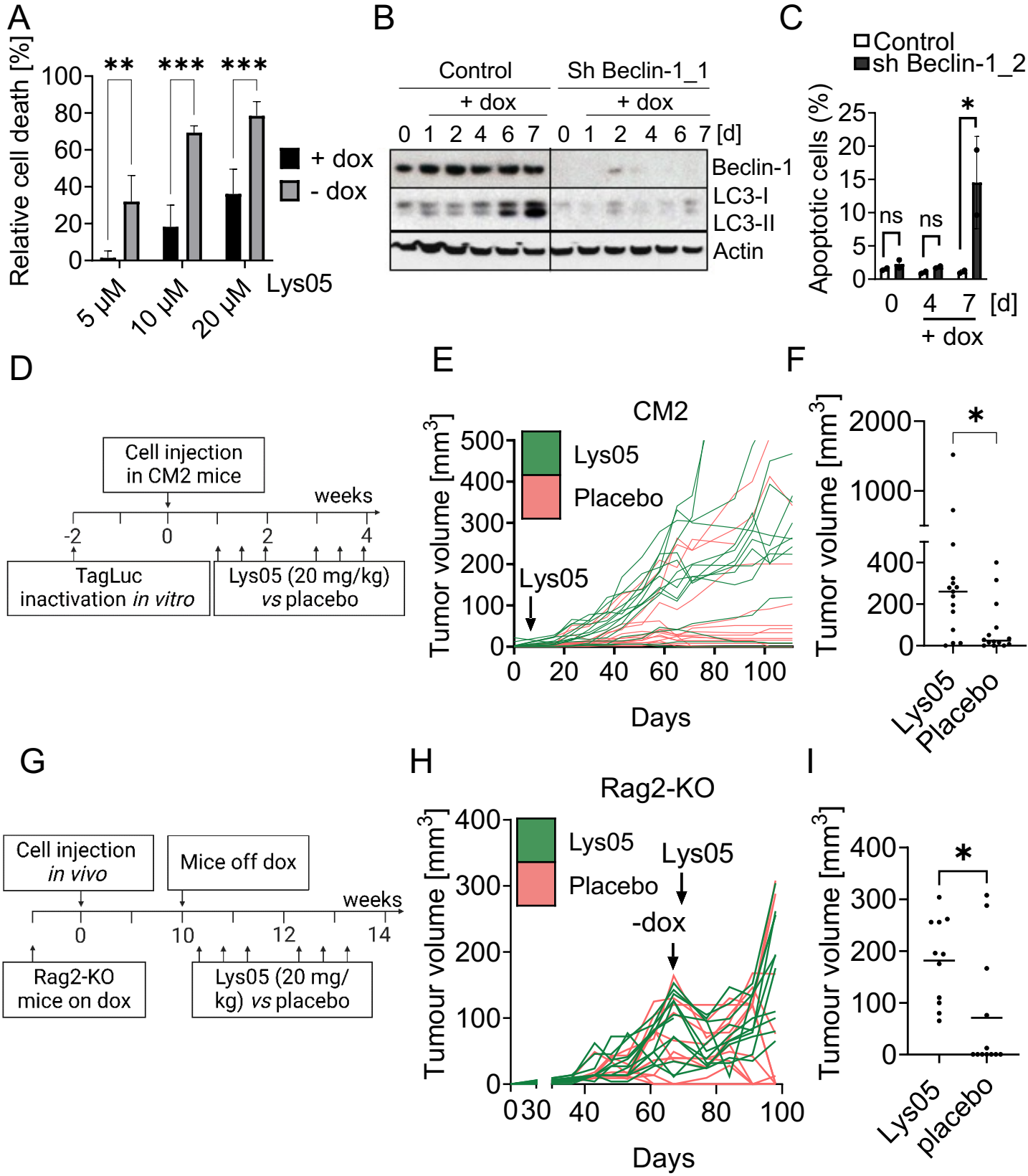
A
Relative cell death [%]
100
80
60
40
20
0
**
***
***
+ dox
- dox
5 µM
10 µM
20 µM
Lys05
B
Control
Sh Beclin-1_1
+ dox
+ dox
0 1 2 4 6 7 0 1 2 4 6 7 [d]
Beclin-1
LC3-I
LC3-II
Actin
C
Control
sh Beclin-1_2
Apoptotic cells (%)
25
20
15
10
5
0
ns
ns
*
0 4 7 [d]
+ dox
D
Cell injection in CM2 mice
weeks
-2
0
2
4
TagLuc inactivation in vitro
Lys05 (20 mg/kg) vs placebo
E
CM2
Tumor volume [mm3]
500
400
300
200
100
0
Lys05
Placebo
Lys05
0 20 40 60 80 100
Days
F
Tumor volume [mm3]
2000
1000
400
200
0
*
Lys05
Placebo
G
Cell injection in vivo
Mice off dox
weeks
0
10
12
14
Rag2-KO mice on dox
Lys05 (20 mg/kg) vs placebo
H
Rag2-KO
Tumour volume [mm3]
400
300
200
100
0
Lys05
Placebo
Lys05
-dox
0 30 40 60 80 100
Days
I
Tumour volume [mm3]
400
300
200
100
0
*
Lys05
placebo
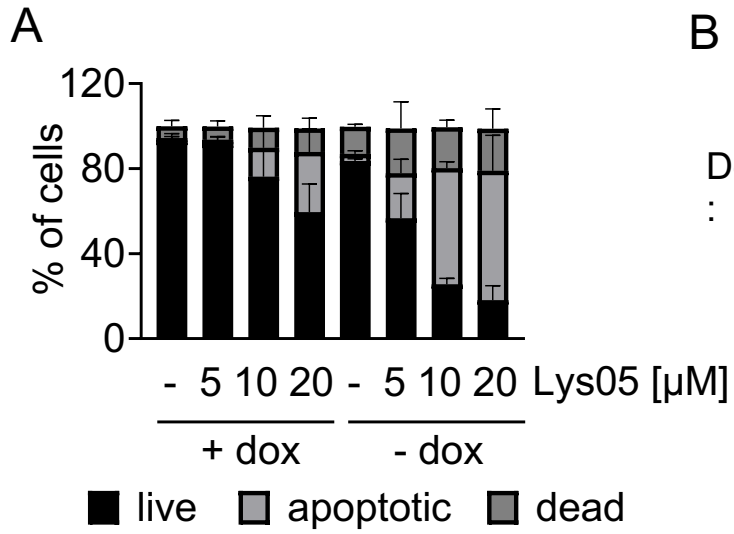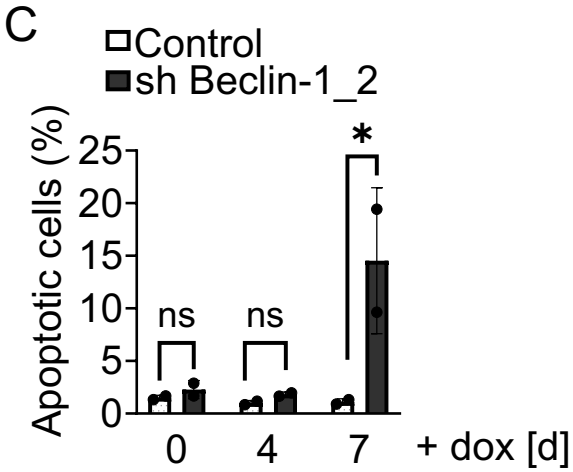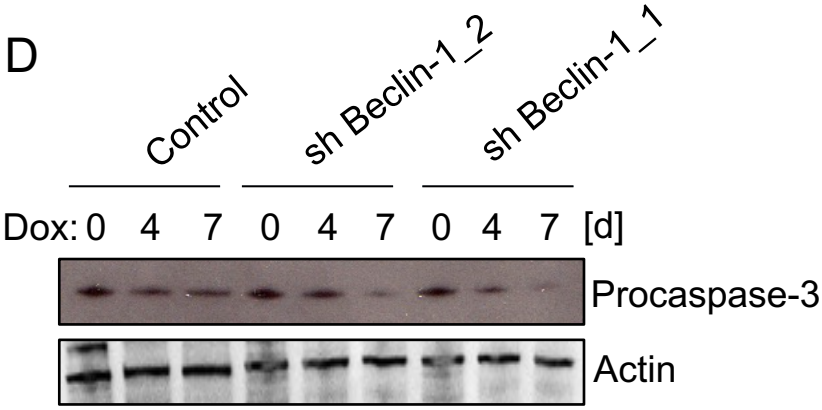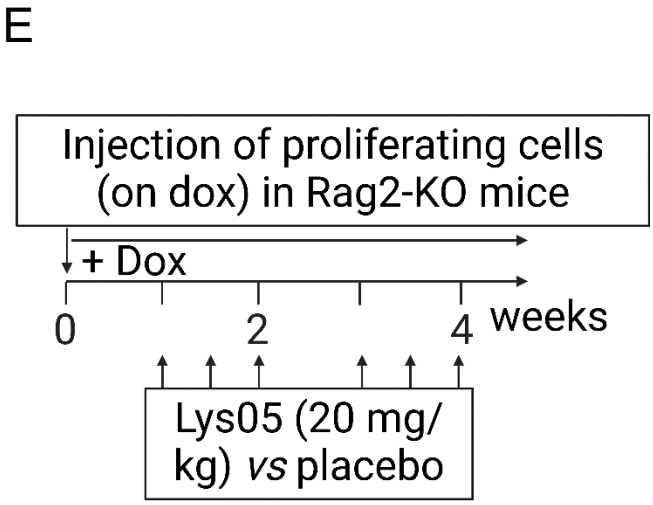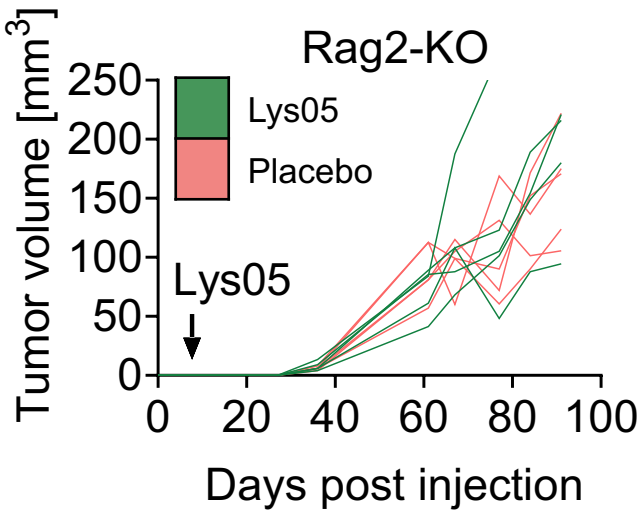
Extended Figure 5